Acta Mech 229, 251–272 (2018)
https://doi.org/10.1007/s00707-017-1968-3

ORIGINAL PAPER

R. Bustamante · K. R. Rajagopal

A nonlinear model for describing the mechanical behaviour of rock

Received: 31 May 2017 / Revised: 24 July 2017 / Published online: 26 September 2017

Abstract In this paper, a nonlinear constitutive relation is proposed to model the behaviour of sandstone. The model is based on a relatively new class of constitutive relations proposed recently in the literature, which cannot be classified as Cauchy or Green elastic bodies. A specific expression for the constitutive relation is proposed on the basis of some experimental data for the compression of a sample of rock, and several boundary value problems are analysed, considering homogeneous distributions of strains, as well as a problem wherein one has a non-homogeneous distribution of strains. Finally, the behaviour of the P- and S-waves is studied for a sample of rock under compression, and it is discovered that the wave speed depends on the compressive load, a result supported by experiments.

1 Introduction

Rock is a material that exhibits nonlinear behaviour in the range of small displacement gradients and hence small strains (see, for example, [1–10]). Traditionally, classical linearized elasticity and plasticity based on the linearized strain have been used to model the behaviour of such materials[1]. In the present communication, we propose a model for the mechanical behaviour of dry rock, which is based on the relatively recent implicit theory for elastic bodies[2] developed by Rajagopal and et al. [22–27]. Consider for instance the implicit constitutive relation

$$\mathfrak{F}(\mathbf{T}, \mathbf{B}) = \mathbf{0}, \tag{1}$$

where $\mathbf{T}$ is the Cauchy stress tensor and $\mathbf{B}$ is the left Cauchy Green tensor. Such a model is appropriate to model isotropic materials (for classification of anisotropy for implicit constitutive relations see [28]) and as rock is invariably anisotropic we need to consider a different class of implicit models. However, as a first step in the development of constitutive relations for rocks, we shall consider the above constitutive relation. The class of models described by (1) contains the interesting new subclass

$$\mathbf{B} = \mathfrak{G}(\mathbf{T}), \tag{2}$$

[1] See, for example, Chapter 11 of [11], Eq. 8.6 of [12], Section 4.8 of [13], Section 9.3 of [7], Eq. 1-2 in [14], Eq. (2.2)(1) in [15,16] and Eq. 5 of [17]. One of the exceptions to this tendency is the nonlinear models proposed by Lyakhovsky and his collaborators, see, for example, [18,19].

[2] As a first approximation in this work, we neglect the dissipation of energy, which is present even for small strains, see, for example, Figs. 1 and 3 in [20] and Section 7 of [21].

R. Bustamante (✉)
Departamento de Ingeniería Mecánica, Universidad de Chile, Beauchef 851, Santiago Centro, Santiago, Chile
E-mail: rogbusta@ing.uchile.cl
Fax: +56-2-26896057

K. R. Rajagopal
Department of Mechanical Engineering, University of Texas A&M, College Station, TX, USA

as well as the classical constitutive equation for the most general class of homogeneous compressible nonlinear Cauchy elastic bodies $\mathbf{T} = \mathfrak{f}(\mathbf{B})$ (see, for example, [29]). When the norm of the gradient of the displacement field is assumed to be very small, we find that $\mathbf{B} \approx 2\boldsymbol{\varepsilon} + \mathbf{I}$, where $\boldsymbol{\varepsilon}$ is the linearized strain tensor, and $\mathbf{I}$ is the identity tensor, respectively. From (2), we obtain the subclass

$$\boldsymbol{\varepsilon} = \mathfrak{H}(\mathbf{T}), \tag{3}$$

which is very important in its own right, and which could be used to study problems, wherein we have elastic bodies that behave nonlinearly even in the case of small strains, such as a variety of metallic alloys, cement and also rock (see [30–32] and the references mentioned therein).

In this study the model (3) is used to fit some experimental data for Berea sandstone, see [2]. In Sect. 2, the equations of kinematics and the general form of the constitutive equations are presented, and some constitutive inequalities are proposed. In Sect. 3, some simple boundary value problems are studied, where we have homogeneous distributions of stresses and strains. In Sect. 4, a specific model is presented to study the behaviour of rock and the strains and stresses within the context of the problems presented in the previous Sect. 3 are determined and plots for the same are documented. In Sect. 5, a boundary value problem where we have non-homogenous distributions of stresses and strains is solved numerically, and the results for the nonlinear model proposed in this study are compared against the prediction of the classical linearized constitutive theory. Finally, in Sect. 6 the incremental analysis presented in [33] is used to obtain the speed of waves for an infinite medium under the effect of compressive loads.

2 Basic equations

2.1 Kinematics and equation of motion

A particle in a body $\mathscr{B}$ is denoted by X, and in the reference configuration it occupies the position $\mathbf{X} = \boldsymbol{\kappa}_R(X)$. The reference configuration is denoted by $\kappa_R(\mathscr{B})$. In the current configuration, the position of the point is denoted by $\mathbf{x}$, and it is assumed that there exists a one-to-one mapping $\boldsymbol{\chi}$ such that $\mathbf{x} = \boldsymbol{\chi}(\mathbf{X}, t)$. The current configuration is denoted by $\kappa_t(\mathscr{B})$. The deformation gradient, the left Cauchy–Green tensor, the displacement vector, and the linearized strain tensor are defined as

$$\mathbf{F} = \frac{\partial \boldsymbol{\chi}}{\partial \mathbf{X}}, \quad \mathbf{B} = \mathbf{F}\mathbf{F}^{\mathrm{T}}, \quad \mathbf{u} = \mathbf{x} - \mathbf{X}, \quad \boldsymbol{\varepsilon} = \frac{1}{2}\left(\frac{\partial \mathbf{u}}{\partial \mathbf{x}} + \frac{\partial \mathbf{u}}{\partial \mathbf{x}}^{\mathrm{T}}\right). \tag{4}$$

The Cauchy stress tensor is denoted by $\mathbf{T}$ and the local form of the balance of linear momentum is

$$\rho \ddot{\mathbf{x}} = \operatorname{div} \mathbf{T} + \rho \mathbf{b}, \tag{5}$$

where ρ is the density of the body and $\mathbf{b}$ represents the specific body forces in the current configuration and where we use the notation $\dot{(\ )}$ for the time derivative. More details concerning the kinematics of deformable bodies and about the balance equations can be found in [34].

2.2 Constitutive relations

The behaviour of rock is modelled by the new constitutive equation (3), under the assumption of the existence of a scalar function $\Pi = \Pi(\mathbf{T})$ such that (see, for example, [35–37])

$$\boldsymbol{\varepsilon} = \frac{\partial \Pi}{\partial \mathbf{T}}. \tag{6}$$

Conditions on Π so that the response is actually elastic have been presented in [37].

If we further assume that the function Π is isotropic, then $\Pi = \Pi(\sigma_1, \sigma_2, \sigma_3)$, where σ_p, $p = 1, 2, 3$ are the eigenvalues of $\mathbf{T}$. The function Π must satisfy the symmetry conditions

$$\Pi(\sigma_1, \sigma_2, \sigma_3) = \Pi(\sigma_2, \sigma_1, \sigma_3) = \Pi(\sigma_1, \sigma_3, \sigma_2). \tag{7}$$

It follows from (6) that

$$\boldsymbol{\varepsilon} = \sum_{p=1}^{3} \frac{\partial \Pi}{\partial \sigma_p} \mathbf{a}^{(p)} \otimes \mathbf{a}^{(p)}, \tag{8}$$

where $\mathbf{a}^{(p)}$ are the eigenvectors of $\mathbf{T}$. If ε_p, $p = 1, 2, 3$ denote the principal strains, from (8) we have

$$\varepsilon_p = \frac{\partial \Pi}{\partial \sigma_p}. \tag{9}$$

The results presented in Sects. 4 and 5 will be compared against the results obtained for the classical linearized model

$$\boldsymbol{\varepsilon} = \frac{(1+\nu)}{E}\mathbf{T} - \frac{\nu}{E}(\mathrm{tr}\mathbf{T})\mathbf{I}, \tag{10}$$

where E and ν are the Young's modulus and the Poisson ratio, respectively.

2.2.1 Constitutive inequalities and some additional restrictions

Some additional restrictions are imposed on the constitutive relation to ensure that the body exhibits reasonable response, the first of such restrictions being a modification of the Baker–Ericksen inequality (see [38] and Section 51 of [29]), which has been already proposed in [39] for the model (2):

$$(\sigma_a - \sigma_b)(\varepsilon_a - \varepsilon_b) > 0, \quad \sigma_a \neq \sigma_b. \tag{11}$$

The above inequality implies that we assume that the directions of the principal strains are the same as the directions of the principal stresses (see (8)). From (9), it follows that the inequality can be rewritten as

$$(\sigma_a - \sigma_b)\left(\frac{\partial \Pi}{\partial \sigma_a} - \frac{\partial \Pi}{\partial \sigma_b}\right) > 0, \quad \sigma_a \neq \sigma_b. \tag{12}$$

In the special case of a body under the influence of a spherical stress $\mathbf{T} = \sigma_S \mathbf{I}$, from (9) we have

$$\varepsilon_S = \frac{\partial \Pi}{\partial \sigma_S}, \tag{13}$$

where ε_S corresponds to the spherical strain produced by σ_S. With the above definitions and results, we can propose another constitutive inequality:

$$(\sigma_S^* - \sigma_S)(\varepsilon_S^* - \varepsilon_S) > 0, \quad \sigma_S^* \neq \sigma_S, \tag{14}$$

which is a modification of the pressure–compression (PC) inequality described in Section 51 of [29].

Finally, if we assume that when $\mathbf{T} = \mathbf{0}$ the body does not have residual strains, then

$$\frac{\partial \Pi}{\partial \sigma_p}(0, 0, 0) = 0, \quad p = 1, 2, 3. \tag{15}$$

2.2.2 A special model

In order to fit some actual experimental data for rock, we propose the following particular expression for Π (this expression below has been used already in [39] for the model (2)):

$$\begin{aligned}\Pi(\sigma_1, \sigma_2, \sigma_3) = {} & \mathfrak{f}_1(\sigma_1) + \mathfrak{f}_1(\sigma_2) + \mathfrak{f}_1(\sigma_3) + \mathfrak{f}_2(\sigma_1)(\sigma_2 + \sigma_3) + \mathfrak{f}_2(\sigma_2)(\sigma_1 + \sigma_3) \\ & + \mathfrak{f}_2(\sigma_3)(\sigma_1 + \sigma_2) + \mathfrak{f}_3\left(\frac{\sigma_1 + \sigma_2 + \sigma_3}{3}\right).\end{aligned} \tag{16}$$

Using (16) in (9), we obtain that

$$\varepsilon_p = \frac{\partial \Pi}{\partial \sigma_p} = \mathfrak{f}_1'(\sigma_p) + \mathfrak{f}_2'(\sigma_p)(\sigma_q + \sigma_r) + \mathfrak{f}_2(\sigma_q) + \mathfrak{f}_2(\sigma_r) + \frac{1}{3}\mathfrak{f}_3'\left(\frac{\sigma_1 + \sigma_2 + \sigma_3}{3}\right), \quad p \neq q \neq r. \tag{17}$$

The second derivatives of Π will be used in Sect. 6 and are listed here

$$\frac{\partial^2 \Pi}{\partial \sigma_p \partial \sigma_s} = \begin{cases} \mathfrak{f}_1''(\sigma_p) + \mathfrak{f}_2''(\sigma_p)(\sigma_q + \sigma_r) + \frac{1}{9}\mathfrak{f}_3''\left(\frac{\sigma_1+\sigma_2+\sigma_3}{3}\right), & p = s, \quad p \neq q \neq r, \\ \mathfrak{f}_2'(\sigma_p) + \mathfrak{f}_2'(\sigma_s) + \frac{1}{9}\mathfrak{f}_3''\left(\frac{\sigma_1+\sigma_2+\sigma_3}{3}\right), & p \neq s. \end{cases} \tag{18}$$

Let us examine briefly the implications of the above model (16). First, we can see that (16) satisfies the symmetry conditions (7), second from (16) we see that the term $\mathfrak{f}_1'(\sigma_p)$ could be used to fit the data from a tension/compression test in a simple manner, while the terms $\mathfrak{f}_2'(\sigma_p)(\sigma_q + \sigma_r) + \mathfrak{f}_2(\sigma_q) + \mathfrak{f}_2(\sigma_r)$ could be used to consider the effect of lateral loads, while the last term $\frac{1}{3}\mathfrak{f}_3'\left(\frac{\sigma_1+\sigma_2+\sigma_3}{3}\right)$ could be used to study the effect of the spherical part of the load on the behaviour of the body.

From (16), we have

$$\frac{\partial \Pi}{\partial \sigma_p}(0,0,0) = \mathfrak{f}_1'(0) + 2\mathfrak{f}_2(0) + \frac{1}{3}\mathfrak{f}_3'(0), \tag{19}$$

and (15) is satisfied if we assume

$$\mathfrak{f}_1'(0) = 0, \quad \mathfrak{f}_2(0) = 0, \quad \mathfrak{f}_3'(0) = 0. \tag{20}$$

3 Boundary value problems: uniform distributions of stresses and strains

In this section, we study briefly some simple boundary value problems, wherein we assume homogeneous distributions of stresses. Some of these problems are considered because they can be used to study some of the experimental data presented in [2].

3.1 Uniform compression/tension of a cylinder without lateral constraints

Here, we are interested in studying the case of a cylindrical sample of rock that is compressed in the axial direction, assuming that the lateral surface is free to expand radially. This is one of the experiments that is routinely performed to study the behaviour of rock [40]. It is necessary to bear in mind that in the actual experiment it is difficult to obtain such uniform distributions of strains, due to end effects (see, for example, [4,5,7,40]).

Let us consider a cylinder that in the undeformed configuration is described in cylindrical coordinates by

$$0 \leq r \leq r_o, \quad 0 \leq \theta \leq 2\pi, \quad 0 \leq z \leq L. \tag{21}$$

Let us assume that this cylinder is deforming under the influence of the stress distribution

$$\mathbf{T} = \sigma_z \mathbf{e}_z \otimes \mathbf{e}_z, \tag{22}$$

where σ_z is constant. In this problem $\sigma_1 = \sigma_z$ and $\sigma_2 = \sigma_r = 0$, $\sigma_3 = \sigma_\theta = 0$ and from (9) we have

$$\varepsilon_z = \left.\frac{\partial \Pi}{\partial \sigma_z}\right|_{(\sigma_z,0,0)}, \quad \varepsilon_r = \varepsilon_\theta = \left.\frac{\partial \Pi}{\partial \sigma_r}\right|_{(\sigma_z,0,0)}. \tag{23}$$

In the special case of (16), we obtain

$$\varepsilon_z = \mathfrak{f}_1'(\sigma_z) + \frac{1}{3}\mathfrak{f}_3'\left(\frac{\sigma_z}{3}\right), \tag{24}$$

$$\varepsilon_r = \varepsilon_\theta = \mathfrak{f}_2(\sigma_z) + \mathfrak{f}_2'(0)\sigma_z + \frac{1}{3}\mathfrak{f}_3'\left(\frac{\sigma_z}{3}\right). \tag{25}$$

Since $\mathbf{T}$ is constant so is $\boldsymbol{\varepsilon}$; therefore, it is possible to obtain $\mathbf{u}$ from (4) $_4$ and the equation of motion (5) (assuming no body forces) is satisfied automatically. The same will be valid for the boundary value problems presented in the following subsections. Notice that when using (6), (9) the radial and axial deformations are obtained directly as functions of the load σ_z.

A restriction on Π can be imposed in view of the above results, namely demanding that when[3] $\sigma_z < 0$ we have $\varepsilon_z < 0$ and $\varepsilon_r > 0$, while if $\sigma_z > 0$ we have $\varepsilon_z > 0$ and $\varepsilon_r < 0$.

Finally, in the case of the classical linearized elastic relation (10) we have

$$\varepsilon_z = \frac{\sigma_z}{E}, \quad \varepsilon_r = -\frac{\nu}{E}\sigma_z. \tag{26}$$

[3] See [39] for the counterpart of these inequalities for the case of large elastic deformations.

3.2 Uniform compression/tension of a cylinder with lateral constraints

For this problem, consider the triaxial compression of a cylindrical sample, where the same cylinder described in (21) is subjected to compression, but where we assume there is a lateral wall that does not allow the cylinder to expand radially, i.e., we have the constraint

$$\varepsilon_r = 0 = \varepsilon_\theta. \tag{27}$$

Because of the above constraint, the presence of an axial compressive stress produces reaction loads in the radial and circumferential directions; therefore, in general we must assume that the stress tensor is of the form

$$\mathbf{T} = \sigma_r \mathbf{e}_r \otimes \mathbf{e}_r + \sigma_\theta \mathbf{e}_\theta \otimes \mathbf{e}_\theta + \sigma_z \mathbf{e}_z \otimes \mathbf{e}_z, \tag{28}$$

where σ_z is given data and σ_r, σ_θ must be found from the constraint (27). Let us take $\sigma_1 = \sigma_z$, $\sigma_2 = \sigma_r$ and $\sigma_3 = \sigma_\theta$ from (9) we have

$$\varepsilon_z = \frac{\partial \Pi}{\partial \sigma_z}, \quad 0 = \frac{\partial \Pi}{\partial \sigma_r}, \quad 0 = \frac{\partial \Pi}{\partial \sigma_\theta}, \tag{29}$$

and it follows from (16) that

$$\varepsilon_z = \mathfrak{f}_1'(\sigma_z) + \mathfrak{f}_2'(\sigma_z)(\sigma_r + \sigma_\theta) + \mathfrak{f}_2(\sigma_r) + \mathfrak{f}_2(\sigma_\theta) + \frac{1}{3}\mathfrak{f}_3'\left(\frac{\sigma_r + \sigma_\theta + \sigma_z}{3}\right), \tag{30}$$

$$0 = \mathfrak{f}_1'(\sigma_r) + \mathfrak{f}_2'(\sigma_r)(\sigma_\theta + \sigma_z) + \mathfrak{f}_2(\sigma_\theta) + \mathfrak{f}_2(\sigma_z) + \frac{1}{3}\mathfrak{f}_3'\left(\frac{\sigma_r + \sigma_\theta + \sigma_z}{3}\right), \tag{31}$$

$$0 = \mathfrak{f}_1'(\sigma_\theta) + \mathfrak{f}_2'(\sigma_\theta)(\sigma_r + \sigma_z) + \mathfrak{f}_2(\sigma_r) + \mathfrak{f}_2(\sigma_z) + \frac{1}{3}\mathfrak{f}_3'\left(\frac{\sigma_r + \sigma_\theta + \sigma_z}{3}\right), \tag{32}$$

and from (31), (32) we see that σ_r and σ_θ should be the same, therefore, if $\sigma_\theta = \sigma_r$ from (30)–(32) we finally obtain

$$\varepsilon_z = \mathfrak{f}_1'(\sigma_z) + 2\mathfrak{f}_2'(\sigma_z)\sigma_r + 2\mathfrak{f}_2(\sigma_r) + \frac{1}{3}\mathfrak{f}_3'\left(\frac{2\sigma_r + \sigma_z}{3}\right), \tag{33}$$

$$0 = \mathfrak{f}_1'(\sigma_r) + \mathfrak{f}_2'(\sigma_r)(\sigma_r + \sigma_z) + \mathfrak{f}_2(\sigma_r) + \mathfrak{f}_2(\sigma_z) + \frac{1}{3}\mathfrak{f}_3'\left(\frac{2\sigma_r + \sigma_z}{3}\right). \tag{34}$$

Eq. (34) should be used to obtain σ_r as a function of σ_z.

A further restriction on the functions $\mathfrak{f}_i$ could be demanded when $\sigma_z = 0$. In this case, from (34) we obtain that

$$0 = \mathfrak{f}_1'(\sigma_r) + \mathfrak{f}_2'(\sigma_r)\sigma_r + \mathfrak{f}_2(\sigma_r) + \frac{1}{3}\mathfrak{f}_3'\left(\frac{2\sigma_r}{3}\right), \tag{35}$$

and it is reasonable that in that case the solution of the above algebraic equation should be $\sigma_r = 0$.

Finally, in the case of the classical linearized elastic relation (10) it is possible to show that

$$\sigma_r = \frac{\nu}{(1-\nu)}\sigma_z, \quad \varepsilon_z = \frac{1}{E}\left[1 - \frac{2\nu^2}{(1-\nu)}\right]\sigma_z. \tag{36}$$

3.3 Triaxial loading of a block

Next, let us work with a block that in the reference configuration is described through

$$-\frac{L_i}{2} \leq x_i \leq \frac{L_i}{2}. \tag{37}$$

This block is assumed to deform under the influence of the stress distribution

$$\mathbf{T} = \sum_{i=1}^{3} \sigma_S \mathbf{e}_i \otimes \mathbf{e}_i, \tag{38}$$

where σ_S is constant. From (9), if $\sigma_j = \sigma_S$, $j = 1, 2, 3$ we have

$$\varepsilon_S = \frac{\partial \Pi}{\partial \sigma_S}, \tag{39}$$

and in the case of (16) the above equation reduces to

$$\varepsilon_S = \mathfrak{f}_1'(\sigma_S) + 2\mathfrak{f}_2'(\sigma_S)\sigma_S + 2\mathfrak{f}_2(\sigma_S) + \frac{1}{3}\mathfrak{f}_3'(\sigma_S), \tag{40}$$

where ε_S would be the strain associated with the above stress.

In the case of the classical linearized elastic relation (10), we have

$$\varepsilon_S = \frac{(1-2\nu)}{E}\sigma_S. \tag{41}$$

3.4 Simple shear of a block

In this problem, we consider the same block described in (37), this time under the influence of the pure shear stress distribution

$$\mathbf{T} = \tau(\mathbf{e}_1 \otimes \mathbf{e}_2 + \mathbf{e}_2 \otimes \mathbf{e}_1), \tag{42}$$

where τ is assumed to be constant.

From (42), we have $\sigma_1 = \tau$, $\sigma_2 = -\tau$ and $\sigma_3 = 0$ and using this in (9) and appealing to (16), we obtain that

$$\frac{\partial \Pi}{\partial \sigma_1} = \mathfrak{f}_1'(\tau) - \mathfrak{f}_2'(\tau)\tau + \mathfrak{f}_2(-\tau), \quad \frac{\partial \Pi}{\partial \sigma_2} = \mathfrak{f}_1'(-\tau) + \mathfrak{f}_2'(-\tau)\tau + \mathfrak{f}_2(\tau), \quad \frac{\partial \Pi}{\partial \sigma_3} = \mathfrak{f}_2(\tau) + \mathfrak{f}_2(-\tau). \tag{43}$$

The eigenvectors of $\mathbf{T}$ are

$$\mathbf{a}^{(1)} = \frac{1}{\sqrt{2}}(\mathbf{e}_1 + \mathbf{e}_2), \quad \mathbf{a}^{(2)} = \frac{1}{\sqrt{2}}(-\mathbf{e}_1 + \mathbf{e}_2), \quad \mathbf{a}^{(3)} = \mathbf{e}_3. \tag{44}$$

Let us assume that a distribution of stress of the form (42) applied on the block described in (37) produces a displacement field of the form

$$u_1 = (\lambda_a - 1)x_1 + \gamma x_2, \quad u_2 = (\lambda_b - 1)x_2, \quad u_3 = (\lambda_c - 1)x_3. \tag{45}$$

In this case, we obtain that

$$\varepsilon_{11} = \lambda_a - 1, \quad \varepsilon_{22} = \lambda_b - 1, \quad \varepsilon_{33} = \lambda_c - 1, \quad \varepsilon_{12} = \frac{\gamma}{2}. \tag{46}$$

Substituting (46) in (8) in view of the above results, we finally obtain that

$$\lambda_a - 1 = \lambda_b - 1 = \frac{1}{2}\{\mathfrak{f}_1'(\tau) + \mathfrak{f}_1'(-\tau) + \mathfrak{f}_2(\tau) + \mathfrak{f}_2(-\tau) + \tau[\mathfrak{f}_2'(-\tau) - \mathfrak{f}_2'(\tau)]\}, \tag{47}$$

$$\lambda_c - 1 = \mathfrak{f}_2(\tau) + \mathfrak{f}_2(-\tau), \tag{48}$$

$$\gamma = \mathfrak{f}_1'(\tau) - \mathfrak{f}_1'(-\tau) + \mathfrak{f}_2(-\tau) - \mathfrak{f}_2(\tau) - \tau[\mathfrak{f}_2'(\tau) + \mathfrak{f}_2'(-\tau)]. \tag{49}$$

In the case of the classical linearized model (10), there is no coupling between the shear stresses and the longitudinal deformations, and we simply have

$$\gamma = \frac{2(1+\nu)}{E}\tau. \tag{50}$$

3.5 Shear and compression of a block

In this last example, let us consider the block described by (37) now under the influence of the stress field

$$\mathbf{T} = \sigma \mathbf{e}_1 \otimes \mathbf{e}_1 + \tau(\mathbf{e}_1 \otimes \mathbf{e}_2 + \mathbf{e}_2 \otimes \mathbf{e}_1). \tag{51}$$

It follows that the principal stresses are

$$\sigma_1 = \frac{1}{2}\left[\sigma + \sqrt{\sigma^2 + 4\tau^2}\right], \quad \sigma_2 = \frac{1}{2}\left[\sigma - \sqrt{\sigma^2 + 4\tau^2}\right], \quad \sigma_3 = 0, \tag{52}$$

and the principal directions are

$$\mathbf{a}^{(1)} = \aleph_1(\ell_1 \mathbf{e}_1 + \mathbf{e}_2), \quad \mathbf{a}^{(2)} = \aleph_2(\ell_2 \mathbf{e}_1 + \mathbf{e}_2), \quad \mathbf{a}^{(3)} = \mathbf{e}_3, \tag{53}$$

where we have defined

$$\aleph_1 = \frac{\sqrt{2}\tau}{\sqrt{\sigma^2 + 4\tau^2 + \sigma\sqrt{\sigma^2 + 4\tau^2}}}, \quad \aleph_2 = \frac{\sqrt{2}\tau}{\sqrt{\sigma^2 + 4\tau^2 - \sigma\sqrt{\sigma^2 + 4\tau^2}}}, \tag{54}$$

$$\ell_1 = \frac{\sigma + \sqrt{\sigma^2 + 4\tau^2}}{2\tau}, \quad \ell_2 = \frac{\sigma - \sqrt{\sigma^2 + 4\tau^2}}{2\tau}. \tag{55}$$

Assuming that the body deforms in the same manner as in (45), from (8) we obtain that

$$\lambda_a - 1 = \frac{\partial \Pi}{\partial \sigma_1}\aleph_1^2 \ell_1^2 + \frac{\partial \Pi}{\partial \sigma_2}\aleph_2^2 \ell_2^2, \tag{56}$$

$$\lambda_b - 1 = \frac{\partial \Pi}{\partial \sigma_1}\aleph_1^2 + \frac{\partial \Pi}{\partial \sigma_2}\aleph_2^2, \tag{57}$$

$$\lambda_c - 1 = \frac{\partial \Pi}{\partial \sigma_3}, \tag{58}$$

$$\gamma = 2\left(\frac{\partial \Pi}{\partial \sigma_1}\aleph_1^2 \ell_1 + \frac{\partial \Pi}{\partial \sigma_2}\aleph_2^2 \ell_2\right), \tag{59}$$

where

$$\frac{\partial \Pi}{\partial \sigma_1} = \mathfrak{f}_1'(\sigma_1) + \mathfrak{f}_2'(\sigma_1)\sigma_2 + \mathfrak{f}_2(\sigma_2) + \frac{1}{3}\mathfrak{f}_3'\left(\frac{\sigma_1 + \sigma_2}{3}\right), \tag{60}$$

$$\frac{\partial \Pi}{\partial \sigma_2} = \mathfrak{f}_1'(\sigma_2) + \mathfrak{f}_2'(\sigma_2)\sigma_1 + \mathfrak{f}_2(\sigma_1) + \frac{1}{3}\mathfrak{f}_3'\left(\frac{\sigma_1 + \sigma_2}{3}\right), \tag{61}$$

where σ_1, σ_2 are given in (52).

Regarding this boundary value problem, we are particularly interested in studying the behaviour of γ in terms of σ, because, as described in detail in the next section, there is some experimental information for the shear modulus as a function of the compressive stress for a cylindrical sample under torsion and compression (see [2]). To obtain such a shear modulus which would depend on the compressive stress, we can start from (59). From (60), (61) and (52) we see that the right side of (59) depends on σ and τ, so let us define the function $\mathcal{H}$ as

$$\mathcal{H}(\sigma, \tau) = 2\left(\frac{\partial \Pi}{\partial \sigma_1}\aleph_1^2 \ell_1 + \frac{\partial \Pi}{\partial \sigma_2}\aleph_2^2 \ell_2\right), \tag{62}$$

then (59) becomes

$$\gamma = \mathcal{H}(\sigma, \tau). \tag{63}$$

For our nonlinear model (63), the shear modulus can be obtained by assuming τ to be very small (in comparison to a given reference value for the stresses), and expressing γ as a Taylor series in τ, retaining only up to linear terms in τ. From (63), we have

$$\gamma \approx \mathcal{H}(\sigma, 0) + \left.\frac{\partial \mathcal{H}}{\partial \tau}\right|_{\tau=0} \tau. \tag{64}$$

Table 1 Constants for the functions presented in (69)

α_1	α_2	α_3	c_1	c_2	c_3	d_1	d_2	d_3
0.011	−0.0004	0.001	−0.08	−0.05	−0.08	0.1	0.2	0.1

From (54) and (55), it is easy to see that $\aleph_1^2 \ell_1 = 0$ and $\aleph_2^2 \ell_2 = 0$ when $\tau = 0$, therefore from (62), $\mathcal{H}(\sigma, 0) = 0$ and from (64) we finally obtain

$$\gamma \approx \left. \frac{\partial \mathcal{H}}{\partial \tau} \right|_{\tau=0} \tau. \tag{65}$$

The shear modulus $G = G(\sigma)$ could be defined as

$$G = \frac{1}{\left. \frac{\partial \mathcal{H}}{\partial \tau} \right|_{\tau=0}}. \tag{66}$$

From (122) (see Appendix A) defining $\sigma = -\vartheta$ with $\vartheta > 0$, we have that

$$\left. \frac{\partial \mathcal{H}}{\partial \tau} \right|_{\tau=0} = 2 \left[\frac{\mathfrak{f}_2(-\vartheta)}{\vartheta} - \frac{\mathfrak{f}_1'(-\vartheta)}{\vartheta} - \mathfrak{f}_2'(0) \right]. \tag{67}$$

4 A model for the mechanical behaviour of rock

The main experimental information to be used in the present study is Figure 4 of [2], where the axial deformation for a sample under compression assuming lateral constraint are documented. From Table 1 of [3], we also have some information concerning the behaviour of different types of rock under tension, where the main result is that most types of rock are less stiff under tension than compression[4]; therefore, one of the main considerations here is that the behaviour of rock will be different in tension and compression, i.e., in general for the different functions that appear in (16) we have

$$\mathfrak{f}(-x) \neq -\mathfrak{f}(x). \tag{68}$$

We propose the following expressions for the functions $\mathfrak{f}_i$ in (16):

$$\mathfrak{f}_1(x) = \alpha_1 \left[d_1^{c_1 x} - c_1 \ln(d_1) x \right], \quad \mathfrak{f}_2(x) = \alpha_2 \left(d_2^{c_2 x} - 1 \right), \quad \mathfrak{f}_3(x) = 3\alpha_3 \left[d_3^{c_3 x} - c_3 \ln(d_3) x \right], \tag{69}$$

where α_i, c_i and d_i, $i = 1, 2, 3$ are constants. The derivatives of the above functions are

$$\mathfrak{f}_1'(x) = \alpha_1 c_1 \ln d_1 \left(d_1^{c_1 x} - 1 \right), \quad \mathfrak{f}_2'(x) = \alpha_2 c_2 \ln(d_2) d_2^{c_2 x}, \quad \mathfrak{f}_3'(x) = 3\alpha_3 c_3 \ln d_3 \left(d_3^{c_3 x} - 1 \right), \tag{70}$$

and it is easy to see that the restrictions (20) are satisfied.

The second derivatives of $\mathfrak{f}_1(x)$ and $\mathfrak{f}_3(x)$ are needed in Sect. 6 and are given as

$$\mathfrak{f}_1''(x) = \alpha_1 c_1^2 (\ln d_1)^2 d_1^{c_1 x}, \quad \mathfrak{f}_3''(x) = 3\alpha_3 c_3^2 (\ln d_3)^2 d_3^{c_3 x}. \tag{71}$$

Considering the results presented in Sect. 3.2 for a cylinder under compression with lateral constraint and the data presented in [2], and based on the discussion of the behaviour of rock under tension [3], the list of constants presented in Table 1 is proposed for the model (69) [see (16)]. In (69), the physical units of c_i, $i = 1, 2, 3$ are of 1/MPa, while the units of α_1 and α_3 are MPa; finally, the constants d_i, $i = 1, 2, 3$ and α_2 do not have units.

Now, regarding the linearized model (10) we obtain the constants by considering (9) and assuming that $|\sigma_i|$, $i = 1, 2, 3$ are very small (compared with a given characteristic value for the stress), in such a case from (9) we have the approximation

$$\varepsilon_p \approx \left. \frac{\partial^2 \Pi}{\partial \sigma_p \partial \sigma_s} \right|_{(0,0,0)} \sigma_s, \tag{72}$$

[4] See also, for example, Fig. 6 of [18] and Figs 1, 3 of [19].

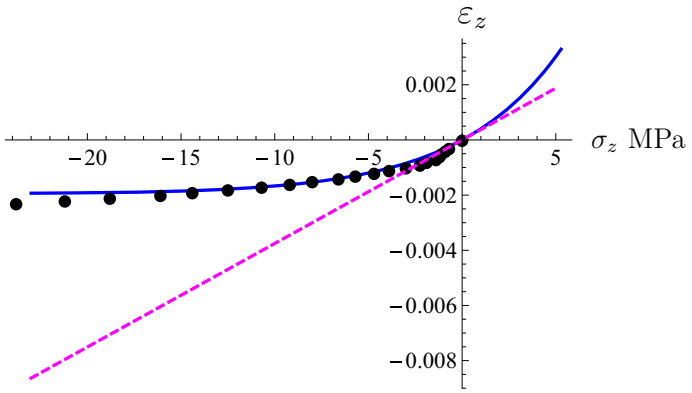

Fig. 1 Compression/tension of a cylinder subject to lateral constraint. The *continuous blue line* shows results for the nonlinear model (16), (69). The *circular black markers* show experimental results taken from Figure 4 of [2] (where results are shown only for compression). The *dashed magenta line* indicates the results for the linearized model (10) considering (75) (color figure online)

where we have used (15) and where from (16) we have

$$\left.\frac{\partial^2 \Pi}{\partial \sigma_p \partial \sigma_s}\right|_{(0,0,0)} = \begin{cases} \mathfrak{f}_1''(0) + \frac{1}{9}\mathfrak{f}_3''(0), & p = s \\ 2\mathfrak{f}_2'(0) + \frac{1}{9}\mathfrak{f}_3''(0), & p \neq s \end{cases} = \begin{cases} \alpha_1 c_1^2 (\ln d_1)^2 + \frac{\alpha_3 c_3^2}{3}(\ln d_3)^2, & p = s \\ 2\alpha_2 c_2 \ln d_2 + \frac{\alpha_3 c_3^2}{3}(\ln d_3)^2, & p \neq s \end{cases} \tag{73}$$

Replacing the above results in (72) and comparing the expression with (10), it is possible to show that

$$E = \frac{1}{\left[\alpha_1 c_1^2 (\ln d_1)^2 + \frac{\alpha_3 c_3^2}{3}(\ln d_3)^2\right]}, \quad \nu = -\frac{\left[2\alpha_2 c_2 \ln d_2 + \frac{\alpha_3 c_3^2}{3}(\ln d_3)^2\right]}{\left[\alpha_1 c_1^2 (\ln d_1)^2 + \frac{\alpha_3 c_3^2}{3}(\ln d_3)^2\right]}, \tag{74}$$

and considering the values for the constants from Table 1 we have

$$E \approx 2600\,\text{MPa}, \quad \nu \approx 0.1038. \tag{75}$$

With regard to some of the plots to be presented in this and in the following sections, we compare the behaviour of the rock by considering (16), (69) and for the linearized model (10) by considering (75).

In the following figures, we portray the behaviour of the cylinders and slabs described in the problems presented in Sect. 3, within the context of the particular expressions for the constitutive functions given above.

In Fig. 1, results are presented for the compression/tension of a cylinder assuming that the lateral surface of the cylinder cannot deform (see Sect. 3.2), results are shown for the axial component of the strain ε_z by comparing the results for our model (16), (69), against the experimental results in Figure 4 of [2].

In Fig. 2, we document the predictions of the model for the radial reaction stress as a function of the axial stress applied on the cylinder. It is necessary to point out that for the model (16), (69) the restriction that is proposed in (35) is satisfied.

In Fig. 3, we present results for the cylinder described in Sect. 3.1, for the model (16), (69), deforming under compression/tension, but now assuming that the lateral wall is free to expand/compress. Results are presented for the axial and the radial components of the strain as functions of the axial stress. From that figure, we see that the restrictions proposed at the end of Sect. 3.1 are satisfied.

In Fig. 4, results are shown for the problem presented in Sect. 3.3 for the deformation of a slab under the influence of a spherical stress.

In Figs. 5 and 6, we see results for the problem presented in Sect. 3.4 in the case of (16), (69). Figure 5 displays the results for the axial stretching/shortening of the slab under shear stress, while in Fig. 6 we provide the results for the shear deformation in terms of the shear stress.

Within the context of (16), (69), let us study the constitutive inequality (12). In the case of (16), the inequality becomes

$$(\sigma_a - \sigma_b)[\mathfrak{f}_1'(\sigma_a) - \mathfrak{f}_1'(\sigma_b) + \mathfrak{f}_2(\sigma_b) - \mathfrak{f}_2(\sigma_a) + \mathfrak{f}_2'(\sigma_a)(\sigma_b + \sigma_c) - \mathfrak{f}_2'(\sigma_b)(\sigma_a + \sigma_c)] > 0, \tag{76}$$

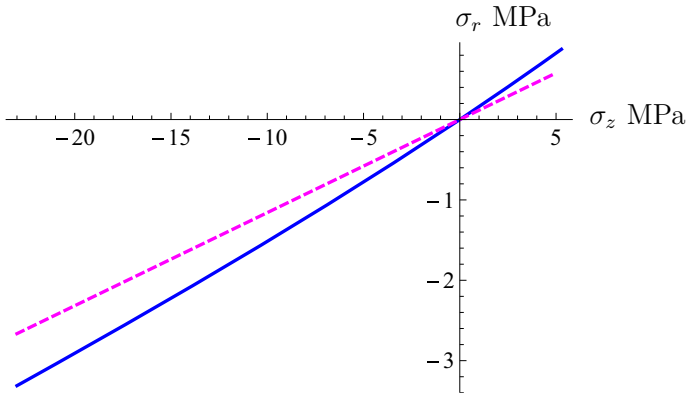

Fig. 2 Compression/tension of a cylinder subject to lateral constraint. The *continuous blue line* shows results for the nonlinear model (16), (69). The *dashed magenta line* shows results for the linearized model (10) (color figure online)

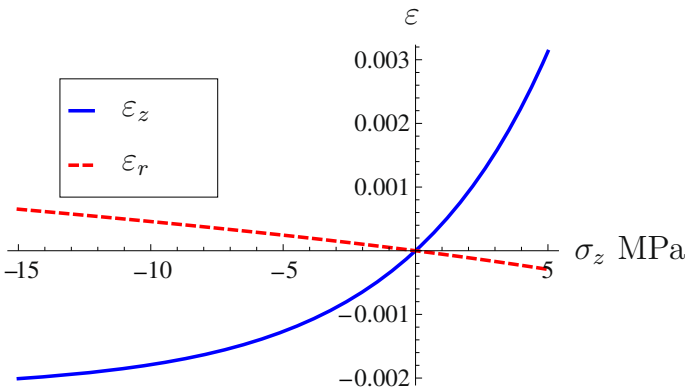

Fig. 3 Axial and radial strains for the case of a cylinder under compression/tension without lateral constraints in the case of the nonlinear model (16), (69)

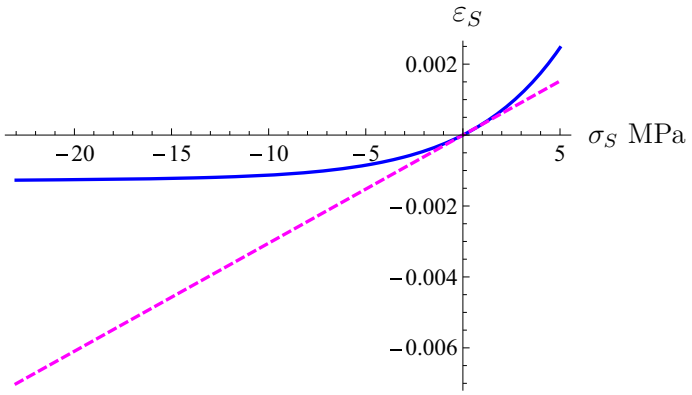

Fig. 4 Strain for the case of a block under the influence of triaxial stress. The *continuous blue line* shows the results for the case of the nonlinear model (16), (69). The *dashed magenta line* presents the results for the linearized model (10) for the values of the constants presented in (75) (color figure online)

which must be true for $\sigma_a \neq \sigma_b$. Now, considering the specific expressions for the functions $\mathfrak{f}_i(x)$, $i = 1, 2, 3$ assumed in (69), and the numerical values of the constants shown in Table 1 that are used to define such functions, it is easy to demonstrate that $(\sigma_a - \sigma_b)[\mathfrak{f}_1'(\sigma_a) - \mathfrak{f}_1'(\sigma_b)] > 0$ and $(\sigma_a - \sigma_b)[\mathfrak{f}_2(\sigma_b) - \mathfrak{f}_2(\sigma_a)] > 0$, however, that is not the case when considering $(\sigma_a - \sigma_b)[\mathfrak{f}_2'(\sigma_a)(\sigma_b + \sigma_c) - \mathfrak{f}_2'(\sigma_b)(\sigma_a + \sigma_c)]$. Therefore, in order to explore if (69) satisfy (76) in Fig. 7 we show contour plots for the function $g(\sigma_a, \sigma_b) = (\sigma_a - \sigma_b)[\mathfrak{f}_1'(\sigma_a) - \mathfrak{f}_1'(\sigma_b) + \mathfrak{f}_2(\sigma_b) - \mathfrak{f}_2(\sigma_a) + \mathfrak{f}_2'(\sigma_a)(\sigma_b + \sigma_c) - \mathfrak{f}_2'(\sigma_b)(\sigma_a + \sigma_c)]$ for some specific values for σ_c,

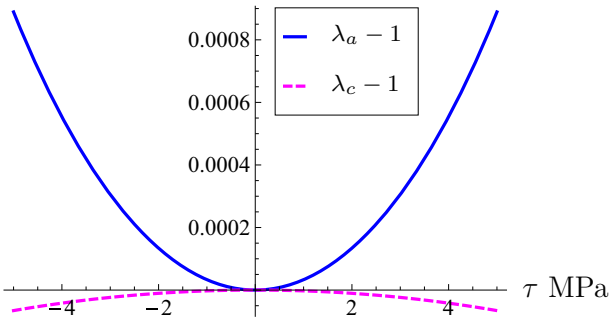

Fig. 5 Shearing of a block. Results for the extension/compression of the block under simple shear within the context of the nonlinear model (16), (69)

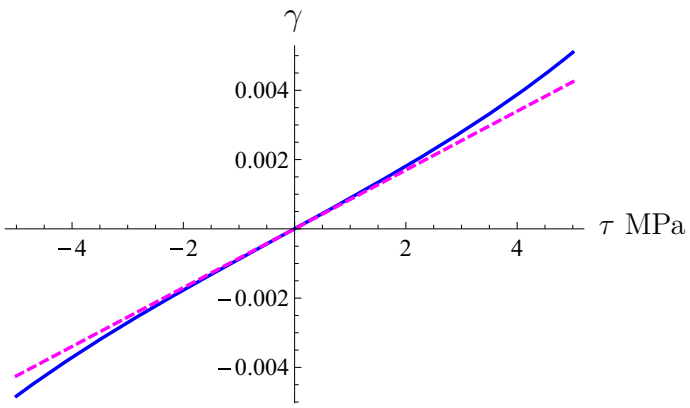

Fig. 6 Results for the shear deformation of a block. The continuous *blue line* shows the results in the case of the nonlinear model (16), (69). The *magenta dashed line* represents the results with regard to the linearized model (10) when (75) (color figure online)

considering a range of values for σ_a and σ_b from -20 to 5 MPa. From such plots, it is possible to observe that for the range of values for σ_a and σ_b, and for the four specific values for σ_c, the function $g(\sigma_a, \sigma_b)$ would be positive and (76) would be satisfied.

Regarding the PC inequality (14), we have not been able to show analytically that such a restriction is satisfied for (16), but by studying contour plots similar to that is shown in Fig. 7 for the range of values for σ_S^* and the σ_S between -23 and 5 MPa, it is possible to see that such an inequality would be satisfied with regard to (69) for the constants presented in Table 1. For brevity, we do not show such plots here.

Finally, in Fig. 8 some results are presented for the case of the shearing of a slab that is also subject to compression that was studied in Sect. 3.5. Specifically, the results for the function $\frac{\partial \mathcal{H}}{\partial \tau}(\vartheta, 0)/\frac{\partial \mathcal{H}}{\partial \tau}(0, 0) = G(\vartheta = 0)/G(\vartheta)$ are depicted (see (67) recalling that $\mathcal{H} = \mathcal{H}(\sigma, \tau)$). These results could be compared with the experimental results obtained from Figure 7 of [2], where the difference in the shear modulus is presented as a function of the compressive stress for a cylinder under compression and torsion.

5 Boundary value problem wherein non-uniform distributions of stresses and strains are considered: expansion–compression of a cylindrical annulus

In this section, we present results for a boundary value problem, wherein the distributions of stresses and strains are inhomogeneous, to study the predictions of the nonlinear model (16), (69), and then compare these results, for some cases, with that for the linearized model (10).

Let us consider a cylindrical annulus that in the undeformed configuration is described through

$$r_i \leq r \leq r_o, \quad 0 \leq \theta \leq 2\pi, \quad 0 \leq z \leq L. \tag{77}$$

This annulus is assumed to be subject to the following distribution of stresses

$$\mathbf{T} = T_{rr}(r)\mathbf{e}_r \otimes \mathbf{e}_r + T_{\theta\theta}(r)\mathbf{e}_\theta \otimes \mathbf{e}_\theta + T_{zz}(r)\mathbf{e}_z \otimes \mathbf{e}_z, \tag{78}$$

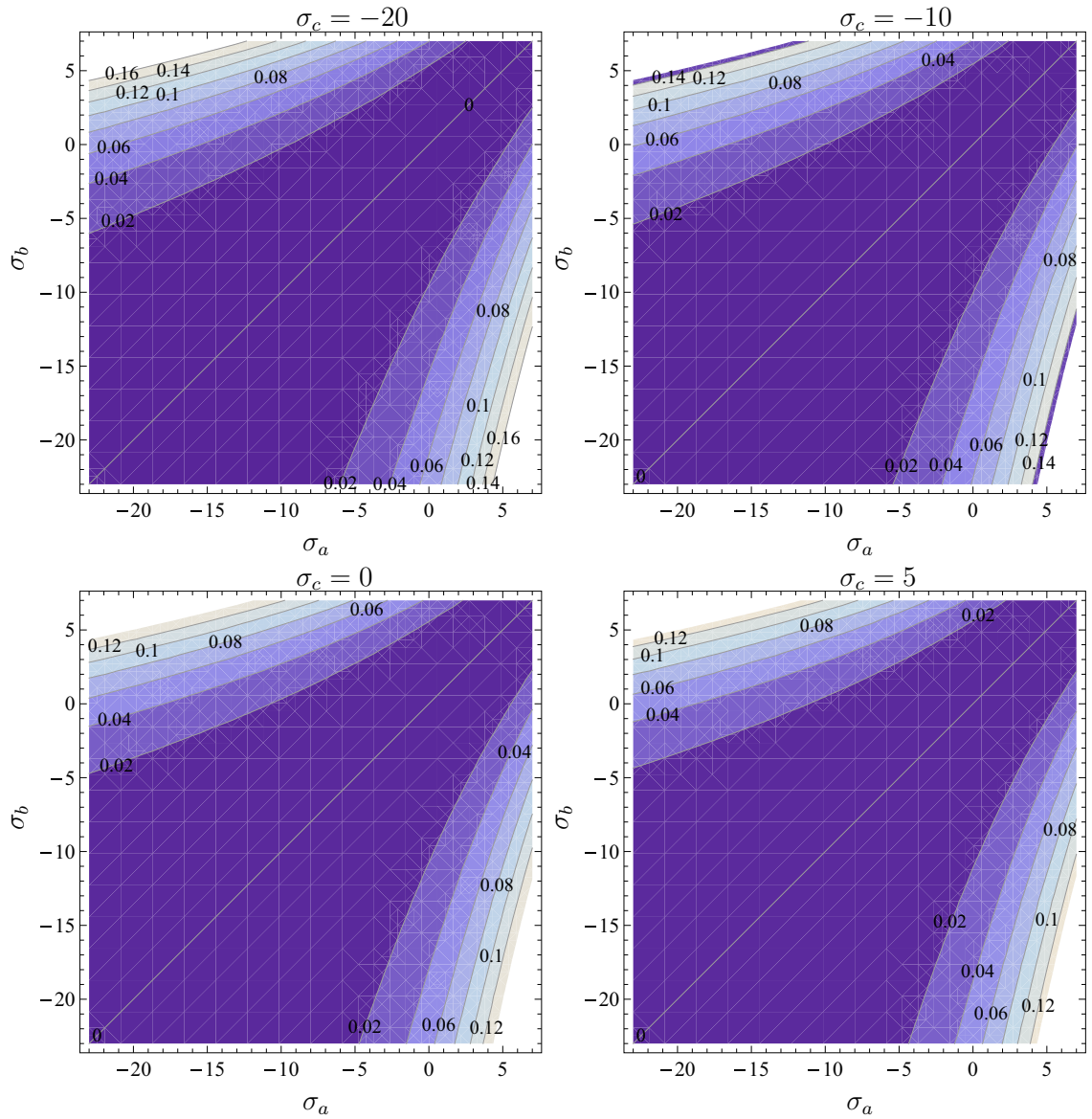

Fig. 7 Contour plots for the function $g(\sigma_a, \sigma_b) = (\sigma_a - \sigma_b)[\mathfrak{f}_1'(\sigma_a) - \mathfrak{f}_1'(\sigma_b) + \mathfrak{f}_2(\sigma_b) - \mathfrak{f}_2(\sigma_a) + \mathfrak{f}_2'(\sigma_a)(\sigma_b + \sigma_c) - \mathfrak{f}_2'(\sigma_b)(\sigma_a + \sigma_c)]$ for different values for σ_c. The stresses are in MPa

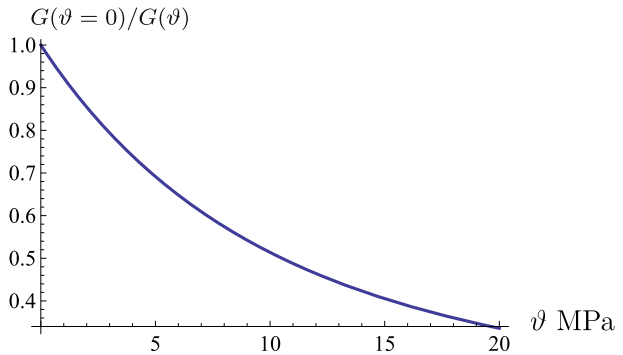

Fig. 8 Dimensionless shear modulus for a slab under the influence of a compressive load, in the case of the nonlinear model (16), (69)

which we assume produces the displacement field (see [36])

$$\mathbf{u} = u_r(r)\mathbf{e}_r + (\lambda - 1)z\mathbf{e}_z, \tag{79}$$

where λ is a positive constant.

For the stress distribution (78), the equilibrium equation becomes

$$T_{\theta\theta} = \frac{\mathrm{d}}{\mathrm{d}r}(rT_{rr}), \tag{80}$$

while from $(4)_4$ and (79) we obtain that

$$\varepsilon_{rr} = \frac{\mathrm{d}u_r}{\mathrm{d}r}, \quad \varepsilon_{\theta\theta} = \frac{u_r}{r}, \quad \varepsilon_{zz} = \lambda - 1. \tag{81}$$

In this problem, we have $\sigma_1 = T_{rr}$, $\sigma_2 = T_{\theta\theta} = \frac{\mathrm{d}}{\mathrm{d}r}(rT_{rr})$, $\sigma_3 = T_{zz}$ and $\varepsilon_1 = \frac{\mathrm{d}u_r}{\mathrm{d}r}$, $\varepsilon_2 = \frac{u_r}{r}$ and $\varepsilon_3 = \lambda - 1$.

From (78), (80), (81) and (9), we have

$$\frac{\mathrm{d}u_r}{\mathrm{d}r} = \frac{\partial\Pi}{\partial\sigma_1}(T_{rr}, T'_{rr}, T_{zz}, r), \quad \frac{u_r}{r} = \frac{\partial\Pi}{\partial\sigma_2}(T_{rr}, T'_{rr}, T_{zz}, r), \quad \lambda - 1 = \frac{\partial\Pi}{\partial\sigma_3}(T_{rr}, T'_{rr}, T_{zz}, r). \tag{82}$$

And from $(82)_{1,2}$, we can obtain that

$$\frac{\mathrm{d}}{\mathrm{d}r}\left(r\frac{\partial\Pi}{\partial\sigma_2}\right) = \frac{\partial\Pi}{\partial\sigma_1}. \tag{83}$$

The above equation and $(82)_3$ should be solved for $T_{rr}(r)$ and $T_{zz}(r)$, where $u_r(r)$ and $T_{\theta\theta}(r)$ are obtained from $u_r(r) = r\frac{\partial\Pi}{\partial\sigma_2}(T_{rr}, T'_{rr}, T_{zz}, r)$ and $T_{\theta\theta} = \frac{\mathrm{d}}{\mathrm{d}r}(rT_{rr})$, respectively.

It has not been possible so far to solve (83) and $(82)_3$ exactly in the case of the nonlinear model (16), (69); therefore, we solve them using the finite element method (see [36]), for which we first take the derivative of $(82)_3$

$$0 = \frac{\mathrm{d}}{\mathrm{d}r}\left(\frac{\partial\Pi}{\partial\sigma_3}\right), \tag{84}$$

and we assume that $T_{zz}(r)$ is given in terms of the auxiliary potential $\tau_{zz}(r)$ as

$$T_{zz}(r) = \frac{\mathrm{d}\tau_{zz}}{\mathrm{d}r}(r). \tag{85}$$

Eqs. (83) and (84) correspond to two nonlinear second-order coupled ordinary differential equations for $T_{rr}(r)$ and $\tau_{zz}(r)$, which are solved using the program Comsol 3.4 [41].

Regarding the boundary conditions, we consider two cases

$$\text{Case A:} \quad T_{rr}(r_i) = -P, \quad T_{rr}(r_o) = 0, \tag{86}$$

$$\text{Case B:} \quad T_{rr}(r_i) = 0, \quad T_{rr}(r_o) = -P, \quad r_o \gg r_i. \tag{87}$$

In the first case A, we are interested in studying the behaviour of an annulus under a radial load applied inside, while in the second case B we are interested in studying the behaviour of a large body with a cylindrical hole under the effect of a far away radial compressive load. In both cases, we assume that $\lambda < 1$, i.e., we assume compression in the axial direction.

The above conditions have to be supplemented with the following boundary conditions when using the finite element method for the nonlinear model (16):

$$\tau_z(r_i) = 0, \quad \lambda - 1 = \frac{\partial\Pi}{\partial\sigma_3}(T_{rr}, T'_{rr}, T_{zz}, r_o)\Big|_{r=r_o}. \tag{88}$$

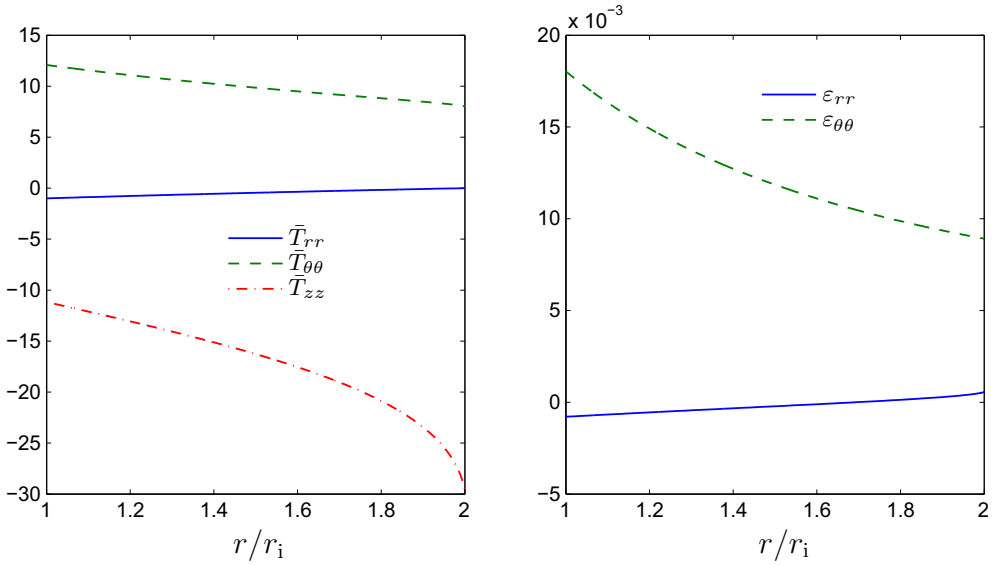

Fig. 9 Distributions of the dimensionless components of the stress and the strain tensors for the boundary condition case A when $P = 1$ MPa and $\lambda = 0.99746$

When considering the linearized model (10), Eqs. (82) can be solved exactly obtaining

$$T_{rr}(r) = C_0 + \frac{C_1}{r^2}, \quad T_{\theta\theta}(r) = C_0 - \frac{C_1}{r^2}, \quad T_{zz}(r) = E(\lambda - 1) + 2\nu C_0, \tag{89}$$

$$\frac{u_r(r)}{r} = \frac{1}{E}\left\{C_0[1 - \nu(1 + 2\nu)] - \frac{C_1}{r^2}(1 + \nu)\right\}, \tag{90}$$

where

$$\text{Case A:} \quad C_0 = \frac{P r_i^2}{(r_o^2 - r_i^2)}, \quad C_1 = \frac{P r_i^2 r_o^2}{(r_o^2 - r_i^2)}, \tag{91}$$

$$\text{Case B:} \quad C_0 = \frac{P r_o^2}{(r_i^2 - r_o^2)}, \quad C_1 = \frac{P r_i^2 r_o^2}{(r_i^2 - r_o^2)}. \tag{92}$$

For the plots presented in Figs. 9, 10, 11, 12, 13 and 14, we shall use the following notation

$$\bar{T}_{rr} = \frac{T_{rr}}{P}, \quad \bar{T}_{\theta\theta} = \frac{T_{\theta\theta}}{P}, \quad \bar{T}_{zz} = \frac{T_{zz}}{P}, \quad \bar{r} = \frac{r}{r_i}, \quad \bar{u}_r = \frac{u_r}{r_i}, \quad \bar{P} = \frac{P}{P_{\max}}. \tag{93}$$

For the case A, we provide plots for $r_i = 0.1$ m, $r_o = 0.2$ m, while for the case B we provide plots for $r_i = 1$ m, $r_o = 100$ m.

For real samples of rock, the maximum strains before failure are in general smaller than the maximum strains that are shown in Figs. 9 and 10, but in the present work we are not concerned with a damage theory for such materials.

In Fig. 9, results are presented for the distributions of the dimensionless components of the stress and the strain tensor as functions of the dimensionless radius $\bar{r}$, solving the differential equations (83), (84), for the case of the boundary conditions A [see (86)], when[5] $P = 1$ MPa and $\lambda = 0.99746$.

Figure 10 presents for the distribution of the dimensionless components of the stress and strain tensors, for the case of the boundary conditions B [see (87)], when $P = 600$ Pa and $\lambda = 0.9985$, which were the maximum and minimum values for P and λ, for which the numerical code converges.

In Fig. 11, a plot of $\bar{u}_r$ evaluated at $\bar{r} = 1$ as a function of $\bar{P}$ is presented, for the boundary conditions, case A [see (86)], where we compare the results obtained for the nonlinear model (16), (69), and the linearized model (10) with Young's modulus given by (75).

[5] The specific value for λ presented here was chosen such that ε_θ, which for this problem is positive, would be 'small' enough that the constitutive theory (6) would be still valid.

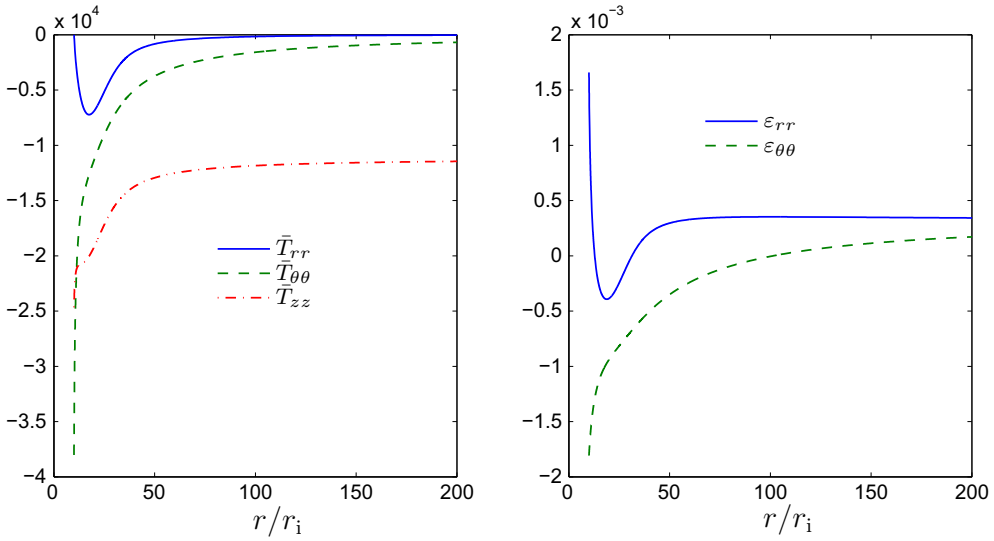

Fig. 10 Distributions of the dimensionless components of the stress and strain tensors for the boundary conditions case B when $P = 600$ Pa and $\lambda = 0.9985$

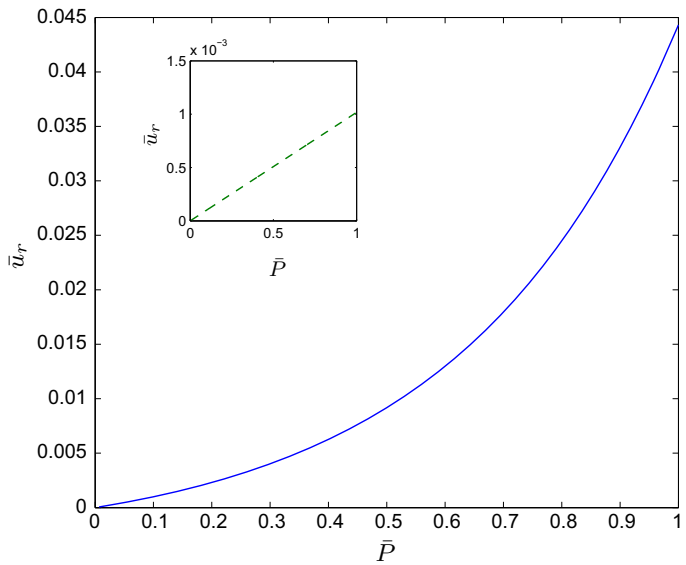

Fig. 11 Dimensionless radial displacement as a function of $\bar{P}$ for the case A. It is assumed that $\lambda = 1$. In the main plot, results are shown for the nonlinear model (16), (69), while in the subplot results are presented in the case of the linearized model (10) when considering (75)

The maximum applied load P was $P_{\max} = 1.5$ MPa. The results for the nonlinear model are one order of magnitude larger than the results for the linearized model (10); therefore, the results are presented in a subplot in the same figure.

In Fig. 12, similar results are presented in the case of the boundary conditions B [see (87)], comparing the results for the nonlinear model (16), (69) with the results of the linearized case (10).

It can be observed that since the compressive load is applied on the outer surface of the body, the dimensionless inner radial displacement is negative, which is the opposite of what is observed in Fig. 11.

In Figs. 13, 14, we provide plots for λ as a function of the total axial force exerted on the tube $\mathcal{F}_z$, which is defined as

$$\mathcal{F}_z = 2\pi \int_{r_i}^{r_o} T_{zz}(r) r \, \mathrm{d}r, \tag{94}$$

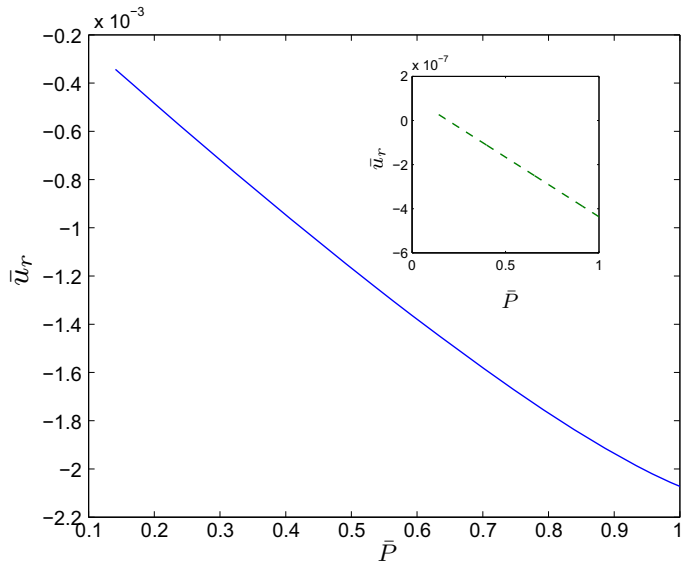

Fig. 12 Dimensionless radial displacement as a function of $\bar{P}$ for the case B, assuming $\lambda = 1$. The main plot shows the results for the nonlinear model, and the subplot we have results for the linearized model

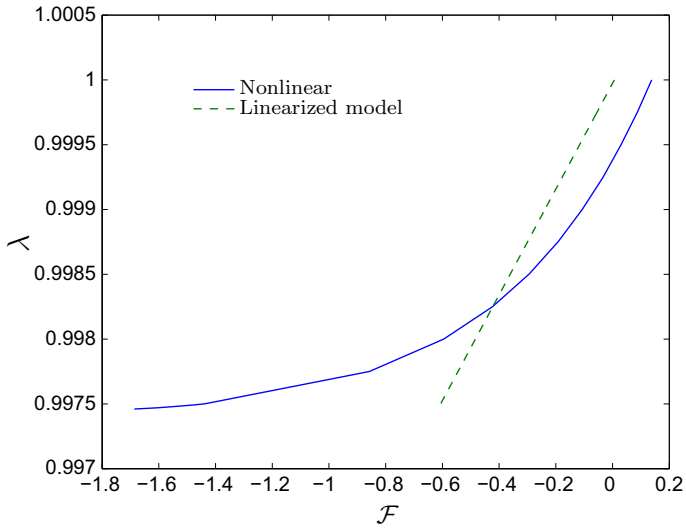

Fig. 13 Axial stretching λ as a function of the total axial force $\mathcal{F}$ (in N) for the case A, assuming $P = 1$ MPa, comparing the results for the linearized model (10) and the nonlinear model (16), (69)

which in the special case of the linearized model (10) in virtue of (94) leads to

$$\mathcal{F}_z = \pi[E(\lambda - 1) + 2\nu C_0](r_o^2 - r_i^2). \tag{95}$$

In Fig. 13 (case A, see (86)), it has been assumed that $P = 1$ MPa, while in Fig. 14 (case B, see (87)) P is assumed to be 600 Pa. In both cases, a comparison between the predictions of the nonlinear model (16), (69) and the linearized model (10) is presented.

6 Propagation of waves of small amplitude

In this section, we study the speed of the S- and P-waves propagating in a sample of rock under compression. First, it is necessary to mention that we have two options for studying the propagation of waves using the model (6):

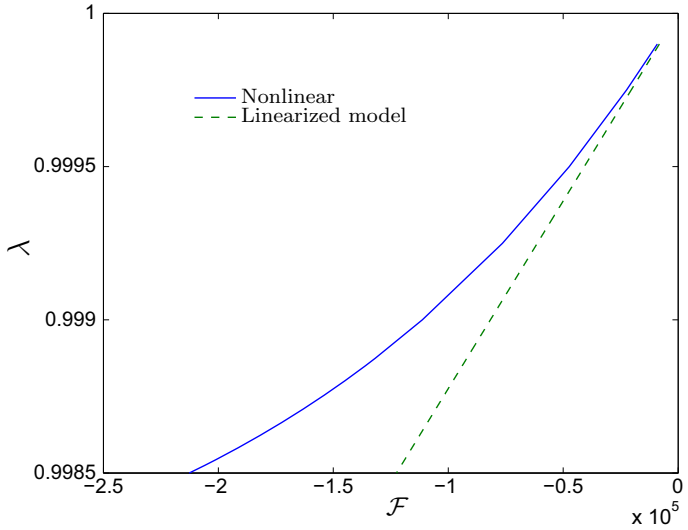

Fig. 14 Axial stretching λ as a function of the total axial force $\mathcal{F}$ (in N) for the case B, assuming $P = 600$ Pa, comparing the results for the linearized and the nonlinear models

- One possibility would be to consider that the amplitude of such waves (for the stress tensor $\mathbf{T}$) is similar or larger in comparison with a characteristic value for the stress, and in such a case we would need to solve in general a complicated system of nonlinear partial differential equations in order to obtain $\mathbf{T}(\mathbf{x}, t)$ and $\mathbf{u}(\mathbf{x}, t)$; such an analysis has been considered, for example, in [42]. In that particular nonlinear case, it is necessary to take into account the fact that quantities such as the frequency and the speed of a wave could depend on the stress, but also could change in time.
- A second simpler option is to suppose that the magnitude of the waves for the stresses is assumed to be very small in comparison with a characteristic stress, and is denoted by $\Delta\mathbf{T}(\mathbf{x}, t)$, superimposed upon a time-independent stress field $\mathbf{T}_o(\mathbf{x})$. In this case, the properties of the wave motion $\Delta\mathbf{u}$ associated with $\Delta\mathbf{T}(\mathbf{x}, t)$ can be obtained by solving some incremental linearized equations. The properties of the wave motion will depend on the time-independent stress distribution $\mathbf{T}_o(\mathbf{x})$. We choose this second method to study the propagation of waves for a rock sample.

Let us briefly present some elements of the incremental analysis within the context of (6) and (8) (see [33]). Let us assume that there is a time-independent distribution of stress $\mathbf{T}_o(\mathbf{x})$ that produces a time-independent displacement field $\mathbf{u}_o(\mathbf{x})$. These two fields are assumed to be solutions of (5) and (6) (see also (8)). A small time-dependent stress $\Delta\mathbf{T}(\mathbf{x}, t)$ is superimposed on the body, and we obtain the total stress field

$$\mathbf{T} = \mathbf{T}_o(\mathbf{x}) + \Delta\mathbf{T}(\mathbf{x}, t), \tag{96}$$

where we assume that $|\Delta\mathbf{T}(\mathbf{x}, t)| \ll |\mathbf{T}_o(\mathbf{x})|$. This small time-dependent stress distribution is assumed to produce a small time-dependent incremental displacement field that is denoted $\Delta\mathbf{u}$. We define a total displacement field $\mathbf{u}$ as $\mathbf{u} = \mathbf{u}_o + \Delta\mathbf{u}$. The key step now is to require that $\mathbf{T} = \mathbf{T}_o(\mathbf{x}) + \Delta\mathbf{T}(\mathbf{x}, t)$ and $\mathbf{u} = \mathbf{u}_o + \Delta\mathbf{u}$ are also solutions of (5) and (6), (8), and since $\mathbf{T}_o(\mathbf{x})$ and $\mathbf{u}_o(\mathbf{x})$ are solutions of (5) and (6), (8) after some manipulations we obtain the incremental equations

$$\operatorname{div}\Delta\mathbf{T} = \rho\frac{\partial^2\Delta\mathbf{u}}{\partial t^2}, \quad \Delta\boldsymbol{\varepsilon} = \boldsymbol{\mathcal{A}}(\mathbf{T}_o)\Delta\mathbf{T}, \tag{97}$$

where we have defined

$$\boldsymbol{\mathcal{A}} = \frac{\partial^2\Pi}{\partial\mathbf{T}\partial\mathbf{T}}. \tag{98}$$

In index notation (Cartesian coordinates), (97) becomes

$$\frac{\partial\Delta T_{ij}}{\partial x_j} = \rho\frac{\partial^2\Delta u_i}{\partial t^2}, \quad \frac{1}{2}\left(\frac{\partial\Delta u_i}{\partial x_j} + \frac{\partial\Delta u_j}{\partial x_i}\right) = \mathcal{A}_{ijkl}\Delta T_{kl}. \tag{99}$$

In the case that $\Pi(\mathbf{T})$ is written in terms of the principal stresses $\Pi = \Pi(\sigma_1, \sigma_2, \sigma_3)$, we have (see [43])

$$\boldsymbol{\mathcal{A}} = \sum_{q=1}^{3}\sum_{p=1}^{3} \frac{1}{2}\frac{\partial^2 \Pi}{\partial\sigma_p \partial\sigma_q}\left(\mathbf{a}^{(p)}\otimes\mathbf{a}^{(p)}\otimes\mathbf{a}^{(q)}\otimes\mathbf{a}^{(q)} + \mathbf{a}^{(q)}\otimes\mathbf{a}^{(q)}\otimes\mathbf{a}^{(p)}\otimes\mathbf{a}^{(p)}\right) + \sum_{p=1}^{3}\frac{\partial\Pi}{\partial\sigma_p}\frac{\partial(\mathbf{a}^{(p)}\otimes\mathbf{a}^{(p)})}{\partial\mathbf{T}}, \tag{100}$$

where

$$\frac{\partial(\mathbf{a}^{(p)}\otimes\mathbf{a}^{(p)})}{\partial\mathbf{T}} = \frac{1}{\sigma_p-\sigma_q}\boldsymbol{\mathcal{Q}}^{(pq)} + \frac{1}{\sigma_p-\sigma_r}\boldsymbol{\mathcal{Q}}^{(pr)}, \quad p\neq q\neq r, \quad p \text{ not summed}, \tag{101}$$

and where

$$\begin{aligned}\boldsymbol{\mathcal{Q}}^{(pq)} = \boldsymbol{\mathcal{Q}}^{(qp)} = \frac{1}{2}(&\mathbf{a}^{(p)}\otimes\mathbf{a}^{(q)}\otimes\mathbf{a}^{(p)}\otimes\mathbf{a}^{(q)} + \mathbf{a}^{(p)}\otimes\mathbf{a}^{(q)}\otimes\mathbf{a}^{(q)}\otimes\mathbf{a}^{(p)}\\ &+\mathbf{a}^{(q)}\otimes\mathbf{a}^{(p)}\otimes\mathbf{a}^{(p)}\otimes\mathbf{a}^{(q)} + \mathbf{a}^{(q)}\otimes\mathbf{a}^{(p)}\otimes\mathbf{a}^{(q)}\otimes\mathbf{a}^{(p)}).\end{aligned} \tag{102}$$

It is possible to show that

$$\mathcal{A}_{ijkl} = \mathcal{A}_{klij} = \mathcal{A}_{jikl} = \mathcal{A}_{ijlk}, \tag{103}$$

which is a consequence of the original definition $\boldsymbol{\mathcal{A}} = \frac{\partial^2\Pi}{\partial\mathbf{T}\partial\mathbf{T}}$.

The system of equations (99) is linear for ΔT_{ij} and Δu_i, but the components of $\mathcal{A}_{ijkl}$ depend on $T_{o_{ij}}$.

Now, considering the solution for $\mathbf{T}_o$ obtained in Sect. 3.2 and presented in Figs. 1, 2, we proceed to solve (99) assuming that media is infinite. To assume that the cylinder is an infinite body in order to solve (99) is an important simplification, but considering the kind of data presented in [2] and in other works (see, for example, [1,40]), such an assumption is important to simplify the problem and to avoid the appearance of reflection of waves at the boundary of the cylinder.

In view of the above remarks, we solve (99) assuming that ΔT_{ij} and Δu_i are given as

$$\Delta T_{ij}(\mathbf{x}, t) = \mathbb{T}_{ij}e^{\iota\omega(s\mathbf{n}\cdot\mathbf{x}-t)}, \quad \Delta u_i(\mathbf{x}, t) = \mathbb{U}_i e^{\iota\omega(s\mathbf{n}\cdot\mathbf{x}-t)}, \tag{104}$$

where $\iota = \sqrt{-1}$ is the imaginary number, ω is the frequency of the wave, s is the slowness and $\mathbf{n}$ is the direction or propagation, and where $\mathbb{T}_{ij}$, $\mathbb{U}_i$ are constant. Substituting the same in (99), we obtain the linear system of equations

$$\begin{pmatrix}
\mathbb{M}_{1,1} & 0 & 0 & \mathbb{M}_{1,4} & \mathbb{M}_{1,5} & 0 & \mathbb{M}_{1,7} & 0 & 0\\
0 & \mathbb{M}_{2,2} & 0 & \mathbb{M}_{2,4} & 0 & \mathbb{M}_{2,6} & 0 & \mathbb{M}_{2,8} & 0\\
0 & 0 & \mathbb{M}_{3,3} & 0 & \mathbb{M}_{3,5} & \mathbb{M}_{3,6} & 0 & 0 & \mathbb{M}_{3,9}\\
\mathbb{M}_{4,1} & \mathbb{M}_{4,2} & \mathbb{M}_{4,3} & \mathbb{M}_{4,4} & \mathbb{M}_{4,5} & \mathbb{M}_{4,6} & \mathbb{M}_{4,7} & 0 & 0\\
\mathbb{M}_{5,1} & \mathbb{M}_{5,2} & \mathbb{M}_{5,3} & \mathbb{M}_{5,4} & \mathbb{M}_{5,5} & \mathbb{M}_{5,6} & 0 & \mathbb{M}_{5,8} & 0\\
\mathbb{M}_{6,1} & \mathbb{M}_{6,2} & \mathbb{M}_{6,3} & \mathbb{M}_{6,4} & \mathbb{M}_{6,5} & \mathbb{M}_{6,6} & 0 & 0 & \mathbb{M}_{6,9}\\
\mathbb{M}_{7,1} & \mathbb{M}_{7,2} & \mathbb{M}_{7,3} & \mathbb{M}_{7,4} & \mathbb{M}_{7,5} & \mathbb{M}_{7,6} & \mathbb{M}_{7,7} & \mathbb{M}_{7,8} & 0\\
\mathbb{M}_{8,1} & \mathbb{M}_{8,2} & \mathbb{M}_{8,3} & \mathbb{M}_{8,4} & \mathbb{M}_{8,5} & \mathbb{M}_{8,6} & \mathbb{M}_{8,7} & 0 & \mathbb{M}_{8,9}\\
\mathbb{M}_{9,1} & \mathbb{M}_{9,2} & \mathbb{M}_{9,3} & \mathbb{M}_{9,4} & \mathbb{M}_{9,5} & \mathbb{M}_{96} & 0 & \mathbb{M}_{9,8} & \mathbb{M}_{9,9}
\end{pmatrix}
\begin{pmatrix}
\mathbb{T}_{11}\\ \mathbb{T}_{22}\\ \mathbb{T}_{33}\\ 2\mathbb{T}_{12}\\ 2\mathbb{T}_{13}\\ 2\mathbb{T}_{23}\\ \mathbb{U}_1\\ \mathbb{U}_2\\ \mathbb{U}_3
\end{pmatrix} =
\begin{pmatrix}
0\\0\\0\\0\\0\\0\\0\\0\\0
\end{pmatrix}, \tag{105}$$

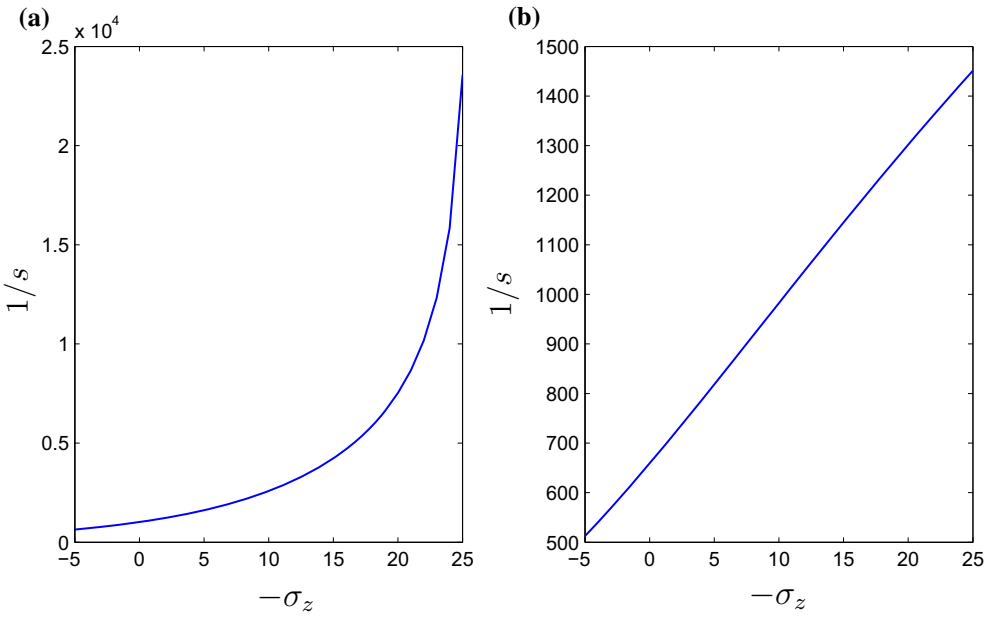

Fig. 15 Results for the wave speed 1/s in m/s as a function of the axial stress $-\sigma_z$ in MPa. In **a** results are shown for the P-wave, and in **b** results are presented for the S-wave

where we have defined

$$\mathbb{M}_{1,1} = \imath s n_1, \quad \mathbb{M}_{1,4} = \frac{\imath s n_2}{2}, \quad \mathbb{M}_{1,5} = \frac{\imath s n_3}{2}, \quad \mathbb{M}_{1,7} = \rho\omega, \tag{106}$$

$$\mathbb{M}_{2,2} = \imath s n_2, \quad \mathbb{M}_{2,4} = \frac{\imath s n_1}{2}, \quad \mathbb{M}_{2,6} = \frac{\imath s n_3}{2}, \quad \mathbb{M}_{2,8} = \rho\omega, \tag{107}$$

$$\mathbb{M}_{3,3} = \imath s n_3, \quad \mathbb{M}_{3,5} = \frac{\imath s n_1}{2}, \quad \mathbb{M}_{3,6} = \frac{\imath s n_2}{2}, \quad \mathbb{M}_{3,9} = \rho\omega, \tag{108}$$

$$\mathbb{M}_{4,1} = \mathcal{A}_{1111}, \quad \mathbb{M}_{4,2} = \mathcal{A}_{1122}, \quad \mathbb{M}_{4,3} = \mathcal{A}_{1133}, \quad \mathbb{M}_{4,4} = \mathcal{A}_{1112}, \quad \mathbb{M}_{4,5} = \mathcal{A}_{1113}, \tag{109}$$

$$\mathbb{M}_{4,6} = \mathcal{A}_{1123}, \quad \mathbb{M}_{4,7} = -n_1 \imath\omega s, \tag{110}$$

$$\mathbb{M}_{5,1} = \mathcal{A}_{1122}, \quad \mathbb{M}_{5,2} = \mathcal{A}_{2222}, \quad \mathbb{M}_{5,3} = \mathcal{A}_{2233}, \quad \mathbb{M}_{5,4} = \mathcal{A}_{2212}, \quad \mathbb{M}_{5,5} = \mathcal{A}_{2213}, \tag{111}$$

$$\mathbb{M}_{5,6} = \mathcal{A}_{2223}, \quad \mathbb{M}_{5,8} = -n_2 \imath\omega s, \tag{112}$$

$$\mathbb{M}_{6,1} = \mathcal{A}_{1133}, \quad \mathbb{M}_{6,2} = \mathcal{A}_{2233}, \quad \mathbb{M}_{6,3} = \mathcal{A}_{3333}, \quad \mathbb{M}_{6,4} = \mathcal{A}_{3312}, \quad \mathbb{M}_{6,5} = \mathcal{A}_{3313}, \tag{113}$$

$$\mathbb{M}_{6,6} = \mathcal{A}_{3323}, \quad \mathbb{M}_{6,9} = -n_3 \imath\omega s, \tag{114}$$

$$\mathbb{M}_{7,1} = \mathcal{A}_{1112}, \quad \mathbb{M}_{7,2} = \mathcal{A}_{2212}, \quad \mathbb{M}_{7,3} = \mathcal{A}_{3312}, \quad \mathbb{M}_{7,4} = \mathcal{A}_{1212}, \quad \mathbb{M}_{7,5} = \mathcal{A}_{1213}, \tag{115}$$

$$\mathbb{M}_{7,6} = \mathcal{A}_{1223}, \quad \mathbb{M}_{7,7} = -\frac{n_2 \imath\omega s}{2}, \quad \mathbb{M}_{7,8} = -\frac{n_1 \imath\omega s}{2}, \tag{116}$$

$$\mathbb{M}_{8,1} = \mathcal{A}_{1113}, \quad \mathbb{M}_{8,2} = \mathcal{A}_{2213}, \quad \mathbb{M}_{8,3} = \mathcal{A}_{3313}, \quad \mathbb{M}_{8,4} = \mathcal{A}_{1213}, \quad \mathbb{M}_{8,5} = \mathcal{A}_{1313}, \tag{117}$$

$$\mathbb{M}_{8,6} = \mathcal{A}_{1323}, \quad \mathbb{M}_{8,7} = -\frac{n_3 \imath\omega s}{2}, \quad \mathbb{M}_{8,9} = -\frac{n_1 \imath\omega s}{2}, \tag{118}$$

$$\mathbb{M}_{9,1} = \mathcal{A}_{1123}, \quad \mathbb{M}_{9,2} = \mathcal{A}_{2223}, \quad \mathbb{M}_{9,3} = \mathcal{A}_{3323}, \quad \mathbb{M}_{9,4} = \mathcal{A}_{1223}, \quad \mathbb{M}_{9,5} = \mathcal{A}_{1323}, \tag{119}$$

$$\mathbb{M}_{9,6} = \mathcal{A}_{2323}, \quad \mathbb{M}_{9,8} = -\frac{n_3 \imath\omega s}{2}, \quad \mathbb{M}_{9,9} = -\frac{n_2 \imath\omega s}{2}, \tag{120}$$

where the expressions for $\mathcal{A}_{ijkl}$ in the case of (16) are computed in Appendix B.

A non-trivial solution of (105) can be found when

$$\det[\mathbb{M}] = 0, \tag{121}$$

where $[\mathbb{M}]$ is the 9×9 matrix with components $\mathbb{M}_{mn}$. From (121), we obtain a polynomial equation for s.

We display the results for the wave speed 1/s for the special case $\mathbf{n} = \mathbf{e}_3$ that is taken to be equal to $\mathbf{e}_z$ (see Sect. 3.2), for different applied external loads σ_z. A wave speed 1/s that is a solution of (121), which is associated with a vector $\mathbb{U}_1 = \mathbb{U}_2 = 0$ and $\mathbb{U}_3 = 1$ could be considered as a P-wave, whereas a solution of (121) for which $\mathbb{U}_3 = 0$ can be considered as a S-wave.

The results shown in Fig. 15 could be compared, at least qualitatively, with the results presented in Figure 5 of [2].

Acknowledgements R. Bustamante would like to express his gratitude for the financial support provided by FONDECYT (Chile) under Grant No. 1160030. K. R. Rajagopal thanks the National Science Foundation and the Office of Naval Research for support of this work. Both authors would like to thank P. Arrue for his help producing the plots presented in Sect. 6.

Appendix A

In this appendix, we derive the form of the derivative of $\mathcal{H}$ with respect to τ that is used in Sect. 3.5. From (62), we have

$$\begin{aligned}\frac{\partial \mathcal{H}}{\partial \tau} = 2\Bigg[&\left(\frac{\partial^2 \Pi}{\partial \sigma_1^2}\frac{\partial \sigma_1}{\partial \tau} + \frac{\partial^2 \Pi}{\partial \sigma_1 \partial \sigma_2}\frac{\partial \sigma_2}{\partial \tau}\right)\aleph_1^2 \ell_1 + \frac{\partial \Pi}{\partial \sigma_1}\left(2\aleph_1 \frac{\partial \aleph_1}{\partial \tau}\ell_1 + \aleph_1^2 \frac{\partial \ell_1}{\partial \tau}\right)\\ &+\left(\frac{\partial^2 \Pi}{\partial \sigma_1 \partial \sigma_2}\frac{\partial \sigma_1}{\partial \tau} + \frac{\partial^2 \Pi}{\partial \sigma_2^2}\frac{\partial \sigma_2}{\partial \tau}\right)\aleph_2^2 \ell_2 + \frac{\partial \Pi}{\partial \sigma_2}\left(2\aleph_2 \frac{\partial \aleph_2}{\partial \tau}\ell_2 + \aleph_2^2 \frac{\partial \ell_2}{\partial \tau}\right)\Bigg],\end{aligned} \tag{122}$$

but from (52), (54) and (55) we have

$$\frac{\partial \sigma_1}{\partial \tau} = \frac{2\tau}{\sqrt{\sigma^2 + 4\tau^2}}, \quad \frac{\partial \sigma_2}{\partial \tau} = -\frac{2\tau}{\sqrt{\sigma^2 + 4\tau^2}}, \tag{123}$$

$$\frac{\partial \aleph_1}{\partial \tau} = \frac{\sqrt{2}\sigma\tau\sqrt{\frac{1}{1-\frac{\sigma}{\sqrt{\sigma^2+4\tau^2}}}}}{(\sigma^2 + 4\tau^2)^{3/2}}, \quad \frac{\partial \aleph_2}{\partial \tau} = -\frac{\sqrt{2}\sigma\tau\sqrt{\frac{1}{1-\frac{\sigma}{\sqrt{\sigma^2+4\tau^2}}}}}{(\sigma^2 + 4\tau^2)^{3/2}}, \tag{124}$$

$$\frac{\partial \ell_1}{\partial \tau} = -\frac{\left(\sigma + \frac{\sigma^2}{\sqrt{\sigma^2+4\tau^2}}\right)}{2\tau^2}, \quad \frac{\partial \ell_2}{\partial \tau} = \frac{\left(-\sigma + \frac{\sigma^2}{\sqrt{\sigma^2+4\tau^2}}\right)}{2\tau^2}. \tag{125}$$

From (123), we note that as $\tau \to 0$ this implies that $\frac{\partial \sigma_1}{\partial \tau} \to 0$ and $\frac{\partial \sigma_2}{\partial \tau} \to 0$. On the other hand, from (124) and (125) we have

$$2\aleph_1 \frac{\partial \aleph_1}{\partial \tau}\ell_1 + \aleph_1^2 \frac{\partial \ell_1}{\partial \tau} = \frac{\sigma^2}{(\sigma^2 + 4\tau^2)^{3/2}}, \quad 2\aleph_2 \frac{\partial \aleph_2}{\partial \tau}\ell_2 + \aleph_2^2 \frac{\partial \ell_2}{\partial \tau} = -\frac{\sigma^2}{(\sigma^2 + 4\tau^2)^{3/2}}, \tag{126}$$

which as $\tau \to 0$ become $\pm\frac{1}{|\sigma|}$, respectively.

If $\tau = 0$, from (52), we find that $\sigma_1 = \frac{1}{2}(\sigma + |\sigma|)$ and $\sigma_2 = \frac{1}{2}(\sigma - |\sigma|)$, then by defining $\sigma = -\vartheta$ with $\vartheta > 0$ we find that $\sigma_1 = 0$ and $\sigma_2 = -\vartheta$. Using all these results when $\tau \to 0$ in (122) and recalling (16), we obtain (67).

Appendix B

In this appendix, we obtain explicit expressions for the components of the tensor $\boldsymbol{\mathcal{A}}$ presented in Sect. 6 (Eq. (100)) in the case of the particular expression for Π presented in (16), for the special case $\mathbf{a}_i = \mathbf{e}_i$, $i = 1, 2, 3$.

In this case, from (100) we obtain that

$$\mathcal{A}_{1111} = \mathfrak{f}_1''(\sigma_1) + \mathfrak{f}_2(\sigma_1)(\sigma_2+\sigma_3) + \frac{1}{9}\mathfrak{f}_3''\left(\frac{\sigma_1+\sigma_2+\sigma_3}{3}\right), \tag{127}$$

$$\mathcal{A}_{2222} = \mathfrak{f}_1''(\sigma_2) + \mathfrak{f}_2(\sigma_2)(\sigma_1+\sigma_3) + \frac{1}{9}\mathfrak{f}_3''\left(\frac{\sigma_1+\sigma_2+\sigma_3}{3}\right), \tag{128}$$

$$\mathcal{A}_{3333} = \mathfrak{f}_1''(\sigma_3) + \mathfrak{f}_2(\sigma_3)(\sigma_1+\sigma_2) + \frac{1}{9}\mathfrak{f}_3''\left(\frac{\sigma_1+\sigma_2+\sigma_3}{3}\right), \tag{129}$$

$$\mathcal{A}_{1122} = \mathfrak{f}_2'(\sigma_1) + \mathfrak{f}_2'(\sigma_2) + \frac{1}{9}\mathfrak{f}_3''\left(\frac{\sigma_1+\sigma_2+\sigma_3}{3}\right), \tag{130}$$

$$\mathcal{A}_{1133} = \mathfrak{f}_2'(\sigma_1) + \mathfrak{f}_2'(\sigma_3) + \frac{1}{9}\mathfrak{f}_3''\left(\frac{\sigma_1+\sigma_2+\sigma_3}{3}\right), \tag{131}$$

$$\mathcal{A}_{2233} = \mathfrak{f}_2'(\sigma_2) + \mathfrak{f}_2'(\sigma_3) + \frac{1}{9}\mathfrak{f}_3''\left(\frac{\sigma_1+\sigma_2+\sigma_3}{3}\right), \tag{132}$$

$$\mathcal{A}_{1212} = \frac{[\mathfrak{f}_2(\sigma_2) - \mathfrak{f}_2(\sigma_1) + \mathfrak{f}_1'(\sigma_1) - \mathfrak{f}_1'(\sigma_2) + (\sigma_2+\sigma_3)\mathfrak{f}_2'(\sigma_1) - (\sigma_1+\sigma_3)\mathfrak{f}_2'(\sigma_2)]}{2(\sigma_1-\sigma_2)}, \tag{133}$$

$$\mathcal{A}_{1313} = \frac{[\mathfrak{f}_2(\sigma_3) - \mathfrak{f}_2(\sigma_1) + \mathfrak{f}_1'(\sigma_1) - \mathfrak{f}_1'(\sigma_3) + (\sigma_2+\sigma_3)\mathfrak{f}_2'(\sigma_1) - (\sigma_1+\sigma_2)\mathfrak{f}_2'(\sigma_3)]}{2(\sigma_1-\sigma_3)}, \tag{134}$$

$$\mathcal{A}_{2323} = \frac{[\mathfrak{f}_2(\sigma_3) - \mathfrak{f}_2(\sigma_2) + \mathfrak{f}_1'(\sigma_2) - \mathfrak{f}_1'(\sigma_3) + (\sigma_1+\sigma_3)\mathfrak{f}_2'(\sigma_2) - (\sigma_1+\sigma_2)\mathfrak{f}_2'(\sigma_3)]}{2(\sigma_2-\sigma_3)}, \tag{135}$$

$$\mathcal{A}_{1112} = 0, \quad \mathcal{A}_{1113} = 0, \quad \mathcal{A}_{1123} = 0, \quad \mathcal{A}_{2212} = 0, \quad \mathcal{A}_{2213} = 0, \quad \mathcal{A}_{2223} = 0, \tag{136}$$

$$\mathcal{A}_{3312} = 0, \quad \mathcal{A}_{3313} = 0, \quad \mathcal{A}_{3323} = 0, \quad \mathcal{A}_{1213} = 0, \quad \mathcal{A}_{1223} = 0, \quad \mathcal{A}_{1323} = 0. \tag{137}$$

If $\sigma_1 \to \sigma_2 = \sigma$, it follows from (133) that

$$\mathcal{A}_{1212} = \frac{1}{2}\left[\mathfrak{f}_1''(\sigma) + (\sigma+\sigma_3)\mathfrak{f}_2''(\sigma) - 2\mathfrak{f}_2'(\sigma)\right]. \tag{138}$$

On the other hand, if $\sigma_1 \to \sigma_3 = \sigma$ from (134) we have

$$\mathcal{A}_{1313} = \frac{1}{2}\left[\mathfrak{f}_1''(\sigma) + (\sigma_2+\sigma)\mathfrak{f}_2''(\sigma) - 2\mathfrak{f}_2'(\sigma)\right]. \tag{139}$$

Finally, if $\sigma_2 \to \sigma_3 = \sigma$ from (135) we obtain that

$$\mathcal{A}_{2323} = \frac{1}{2}\left[\mathfrak{f}_1''(\sigma) + (\sigma_1+\sigma)\mathfrak{f}_2''(\sigma) - 2\mathfrak{f}_2'(\sigma)\right]. \tag{140}$$

References

1. Guyer, R.A., Johnson, P.A.: Nonlinear Mesoscopic Elasticity: The Complex Behaviour of Granular Media Including Rocks and Soil. Wiley-VCH Verlag GmbH & Co. KGaA, Weinheim (2009)
2. Johnson, P.A., Rasolofosaon, P.N.J.: Manifestation of nonlinear elasticity in rock: convincing evidence over large frequency and strain intervals from laboratory studies. Nonlinear Process. Geophys. **3**, 77–88 (1996)
3. Haimson, B.C., Tharp, B.C.: Stresses around boreholes in bilinear elastic rock. In: Paper SPE2141, SPE-AIME Sixth Conference on Drilling and Rock Mechanics, Austin Texas, American Institute of Mining, Metallurgical, and Petroleum Engineers, Inc., pp. 145–151 (1974)
4. Hoek, E.: The development of rock engineering. In: Practical Rock Engineering. www.rocscience.com (2007)
5. Hudson, J.A., Harrison, J.P.: Engineering Rock Mechanics: An Introduction to the Principles. Pergamon, Oxford (1997)
6. Peltzer, G., Crampé, F., King, G.: Evidence of nonlinear elasticity of the crust from the Mw7.6 Mayi (Tibet) earthquake. Science **286**, 272–276 (1999)
7. Lama, R.D., Vutukuri, V.S.: Handbook on Mechanical Properties of Rocks: Testing Techniques and Results, vol. III. Trans. Tech Publications, Zürich (1978)
8. Tutuncu, A.N., Podio, A.L., Sharma, M.M.: Nonlinear viscoelastic behavior of sedimentary rocks, part II: hysteresis effects and influence of type of fluid on elastic moduli. Geophysics **63**, 195–203 (1998)

9. Görte, U.J., Nagel, T., Kolditz, O.: On the necessity and a generalized conceptual model for the consideration of large strains in rock mechanics. In: Idelpsohn, S., Papadrakakis, M. (eds.) Computational Methods for Coupled Problems in Science and Engineering V. A Conference Celebrating the 60th Birthday of Eugenio Oñate, Santa Eulalia, Ibiza, Spain, pp. 80–91, 17–19 June (2013)
10. Paterson, M.S., Olgaard, D.L.: Rock deformation tests to large shear strains in torsion. J. Struct. Geol. **22**, 1341–1358 (2000)
11. Truchaninov, I.A., Iofis, M.A., Kasparian, E.V.: Principles of Rock Mechanics. Terraspace Inc., Rockville (1979)
12. Stagg, K.G., Zienkiewicz, O.C.: Rock Mechanics in Engineering Practice. Wiley, Hoboken (1968)
13. Asszonyi, C., Richten, R.: The Continuum Theory of Rock Mechanics. Trans. Tech. Publications, Zürich (1979)
14. Cowie, P.A., Scholz, C.H.: Physical explanation for the displacement-length relationship of faults using a post-yield fracture mechanics model. J. Struct. Geol. **14**, 1133–1148 (1992)
15. Dragon, A., Mróz, Z.: A continuum model for plastic-brittle behaviour of rock and concrete. Int. J. Eng. Sci. **17**, 121–137 (1979)
16. Poulos, H.G., Davis, E.H.: Elasic Solutions for Soil and Rock Mechanics. Wiley, Hoboken (1974)
17. Fliss, S., Bhat, H.S., Dmowska, R., Rice, J.R.: Fault branching and rupture directivity. J. Geophys. Res. **110**, B06312 (2005)
18. Lyakhovsky, V., Reches, Z., Weinberger, R.: Nonlinear viscoelastic behavior of sedimentary rocks, part II: hysteresis effects and influence of type of fluid on elastic moduli. Geophysics **63**, 195–203 (1998)
19. Lyakhovsky, V., Hamiel, Y., AMpuero, J.P., Ben-Zion, Y.: Nonlinear damage rheology and wave resonance in rocks. Geophysics **178**, 910–920 (2009)
20. Ashby, M.F., Hallan, S.D.: The failure of brittle solids containing small cracks under compressive stress states. Acta Metall. **34**, 497–510 (1986)
21. Aydin, A., Borja, R.I., Eichhubl, P.: Geological and mathematical framework for failure modes in granular rock. J. Struct. Geol. **28**, 83–98 (2006)
22. Rajagopal, K.R.: On implicit constitutive theories. Appl. Math. **48**, 279–319 (2003)
23. Rajagopal, K.R.: The elasticity of elasticity. Z. für Angew. Math. Phys. **58**, 309–317 (2007)
24. Rajagopal, K.R., Srinivasa, A.R.: On the response of non-dissipative solids. Proc. R. Soc. A **463**, 357–367 (2007)
25. Rajagopal, K.R., Srinivasa, A.R.: On a class of non-dissipative solids that are not hyperelastic. Proc. R. Soc. A **465**, 493–500 (2009)
26. Rajagopal, K.R.: On a new class of models in elasticity. Math. Comput. Appl. **15**, 506–528 (2010)
27. Rajagopal, K.R.: Conspectus of concepts of elasticity. Math. Mech. Solids **16**, 536–562 (2011)
28. Rajagopal, K.R.: A note on the classification of anisotropy of bodies defined by implicit constitutive relations. Mech. Res. Commun. **64**, 38–41 (2015)
29. Truesdell, C.A., Noll, W.: The non-linear field theories of mechanics, 3rd edn. Springer, Berlin (2004)
30. Bustamante, R.: Some topics on a new class of elastic bodies. Proc. R. Soc. A **465**, 1377–1392 (2009)
31. Bustamante, R., Rajagopal, K.R.: A note on plain strain and stress problems for a new class of elastic bodies. Math. Mech. Solids **15**, 229–238 (2010)
32. Rajagopal, K.R.: On the nonlinear elastic response of bodies in the small strain range. Acta Mech. **225**, 1545–1553 (2014)
33. Arrue, P., Bustamante, R., Sfyris, S.: A note on incremental equations for a new class of constitutive relations for elastic bodies. Wave Motion **65**, 44–54 (2016)
34. Truesdell, C.A., Toupin, R.: The classical field theories. In: Flügge, S. (ed.) Handbuch der Physik, vol. III/I. Springer, Berlin pp. 226–902 (1960)
35. Bustamante, R., Rajagopal, K.R.: Solutions of some simple boundary value problems within the context of a new class of elastic materials. Int. J. Nonlinear Mech. **46**, 376–386 (2011)
36. Bustamante, R., Rajagopal, K.R.: Solutions of some boundary value problems for a new class of elastic bodies. Comparison with the classical theory of linear elasticity: part I. Problems with cylindrical symmetry. Acta Mech. **226**, 1815–1838 (2015)
37. Bustamante, R., Rajagopal, K.R.: A note on some new classes of constitutive relations for elastic bodies. IMA J. Appl. Math. **80**, 1287–1299 (2015)
38. Baker, M., Ericksen, J.L.: Inequalities restricting the form of the stress-deformation relations for isotropic elastic solids and Reiner–Rivlin fluids. J. Wash. Acad. Sci. **44**, 33–35 (1954)
39. Bustamante, R.: Solutions of some boundary value problems for a class of constitutive relations for non-linear elastic bodies that is not Green elastic. Q. J. Mech. Appl. Math. **69**, 257–279 (2016)
40. Mogi, K.: Experimental Rock Mechanics. Taylor & Francis, London (2007)
41. Comsol Multiphysics, Version 3.4, Comsol Inc. Palo Alto, CA (2007)
42. Bustamante, R., Sfyris, D.: Direct determination of stresses from the stress equations of motion and wave propagation for a new class of elastic bodies. Math. Mech. Solids **20**, 80–91 (2015)
43. Shariff, M.H.B.M.: Spectral derivatives in continuum mechanics Q. Jl. Mech. Appl. Math. doi:10.1093/qjmam/hbx014